


Projected sea-level contributions from tidewater glaciers are highly sensitive to chosen bedrock topography: a case study at Hansbreen, Svalbard

Journal Article

Author(s):

Möller, Marco; Navarro, Francisco; [Huss, Matthias](#) ; Marzeion, Ben

Publication date:

2023-08

Permanent link:

<https://doi.org/10.3929/ethz-b-000596864>

Rights / license:

[Creative Commons Attribution 4.0 International](#)

Originally published in:

Journal of Glaciology 69(276), <https://doi.org/10.1017/jog.2022.117>



Article

Cite this article: Möller M, Navarro F, Huss M, Marzeion B (2023). Projected sea-level contributions from tidewater glaciers are highly sensitive to chosen bedrock topography: a case study at Hansbreen, Svalbard. *Journal of Glaciology* 69(276), 966–980. <https://doi.org/10.1017/jog.2022.117>

Received: 30 August 2022
Revised: 18 November 2022
Accepted: 5 December 2022
First published online: 16 January 2023

Key words:

Arctic glaciology; glacier calving; glacier fluctuations; glacier modelling

Author for correspondence:

Marco Möller,
E-mail: marco.moeller@uni-bremen.de

Projected sea-level contributions from tidewater glaciers are highly sensitive to chosen bedrock topography: a case study at Hansbreen, Svalbard

Marco Möller^{1,2,3} , Francisco Navarro⁴ , Matthias Huss^{5,6,7} 
and Ben Marzeion^{1,2}

¹Institute of Geography, University of Bremen, Bremen, Germany; ²MARUM – Center for Marine Environmental Sciences, University of Bremen, Bremen, Germany; ³Geography Department, Humboldt Universität zu Berlin, Berlin, Germany; ⁴Department of Mathematics Applied to ICT, ETSI de Telecomunicación, Universidad Politécnica de Madrid, Madrid, Spain; ⁵Laboratory of Hydraulics, Hydrology and Glaciology (VAW), ETH Zurich, Zurich, Switzerland; ⁶Swiss Federal Institute for Forest, Snow and Landscape Research (WSL), Birmensdorf, Switzerland and ⁷Department of Geosciences, University of Fribourg, Fribourg, Switzerland

Abstract

Calculation of the calving loss of tidewater glaciers depends on accurate bedrock information. In regional to global-scale projections of future tidewater glacier evolution this dependence is problematic. Bedrock topographies are often unknown and can only be modelled from surface properties. Existing approaches, however, mostly underestimate the ice thickness towards the calving fronts of marine-terminating glaciers. This implies a compromised performance of global-scale projection models which often employ functions of water depth at the calving fronts of tidewater glaciers. Here, we present a sensitivity study that analyses the impact of five different bedrock datasets on projected mass losses from the tidewater glacier Hansbreen in southern Svalbard. Our modelling study calculates the glacier's response to artificial mass-balance forcing. We show that bedrock inaccuracies may lead to a substantially deviating retreat behaviour. The common underestimation of frontal ice thickness/water depth in the modelled bedrock datasets induces an underestimation of sea level-relevant mass losses over the first several decades of modelling. The duration of this period is reduced when assuming warmer climates. Our results thus underline the importance of accurate bedrock topography data for the reliability of glacier evolution projections and for the accuracy of the temporal trajectories of related sea level-relevant mass losses.

Introduction

Tidewater glaciers contributed disproportionately little to sea-level rise over the past two decades (Hugonnet and others, 2021), but are suggested to be among the most important contributors to sea-level rise in the 21st century (Moore and others, 2013). They are also assumed to be a major source of uncertainty in future projections (Luckman and others, 2015). Mass loss by ice discharge from these glaciers is constrained by ice flow velocity and ice thickness at their marine-terminating fronts (e.g. Sánchez-Gómez and others, 2019; Mankoff and others, 2020). Hence, reliable model-based estimates of ice discharge from tidewater glaciers depend to a large extent on accurate bedrock topography data. In spite of recent advances in ice thickness radar and fjord bathymetry measurements worldwide (GlaThiDa Consortium, 2019; Welty and others, 2020; Jakobsson and Mayer, 2022), a widespread lack of measured bedrock and sea floor information continues to exist (Farinotti and others, 2019; Jakobsson and Mayer, 2022), and makes studies of regional to global-scale sea-level contribution from tidewater glaciers predominantly dependent on modelled ice thickness (e.g. Huss and Hock, 2015; Maussion and others, 2019). This dependence introduces substantial uncertainty into modelled regional to global-scale ice discharge numbers and thus into sea-level contributions from tidewater glaciers in general.

Regional to global-scale ice thickness models mostly assume a closed surface mass budget that is locally balanced by the divergence of the ice flux (e.g. Farinotti and others, 2009, 2017, 2019; Huss and Farinotti, 2012; Linsbauer and others, 2012; Rabatel and others, 2018). This assumption is valid for land-terminating glaciers, but problematic for tidewater glaciers, because mass loss by ice discharge would be needed to compensate for surface mass balance across the model domain. Not adequately capturing or even ignoring mass loss by frontal ablation at the glacier terminus thus leads to an underestimation of the ice flux in the lower part of the tongue and thus to an increasing underestimation of ice thickness towards the terminus and generally higher uncertainties in this part of the glacier (Recinos and others, 2019). To overcome this limitation, efforts have been undertaken to account for extensive observational bedrock data or remote-sensing-based flux estimates in regional to global-scale ice thickness models which resulted in more accurate bedrock topography data for tidewater glaciers (McNabb and others, 2015; Fürst and others, 2018; Recinos and others, 2021; Millan and others, 2022).

© The Author(s), 2023. Published by Cambridge University Press on behalf of The International Glaciological Society. This is an Open Access article, distributed under the terms of the Creative Commons Attribution licence (<http://creativecommons.org/licenses/by/4.0/>), which permits unrestricted re-use, distribution and reproduction, provided the original article is properly cited.



Existing global-scale projections of future glacier evolution (Hock and others, 2019; Marzeion and others, 2020) have so far not accounted for these improved methods, and consequently the included shares of mass loss from tidewater glaciers have to be deemed erroneous as they most likely underestimate the occurring ice discharge. This implies considerable overall uncertainty, as tidewater glaciers account for 40% of the area of global glaciers and ice caps outside the two ice sheets (Hugonnet and others, 2021).

Limitations regarding the type of ice discharge models which are applicable in such regional to global-scale studies further add to this uncertainty. In general, ice discharge is the sum of calving flux and the mass flux implied by changes in the position of the calving front (Cogley and others, 2011). Calving processes at the fronts of individual tidewater glaciers can be modelled by a variety of approaches that are mostly physics-based and rely on detailed data and adequate assumptions of physical parameters to achieve reliable results (Benn and others, 2007; Benn and Åström, 2018). This limits their applicability to well-studied glaciers with sufficient observational data. On regional or global scales, however, a different approach is needed. In such alternative models, mass loss by ice discharge can be parameterized by empirically calibrated equations based on water depth and ice thickness data (e.g. Brown and others, 1982; Hanson and Hooke, 2000; Oerlemans and Nick, 2005; Recinos and others, 2021). In order to more adequately capture the retreat of the marine-terminating glacier tongues over time, these models may be refined by an approach based on a flotation criterion. This type of approach limits the length of the glacier to a certain threshold thickness, which is related to buoyancy conditions at the tongue via an empirical parameter (van der Veen, 1996; Vieli and others, 2001).

In any case, regional to global-scale tidewater glacier modelling can be suspected to most crucially depend on the accuracy of bedrock topography data. In order to apply a flotation criterion approach refinement, it is also necessary to additionally constrain the parameters involved in a reasonable way. Bedrock topography influences the ice thickness at the calving front and thus controls the dimension of the flux gate and the strength of the buoyancy forces across the lower tongue (Benn and others, 2007). Modelling experiments with idealized bedrock shapes have shown that, under equal external forcing, a marine-terminating glacier tongue might experience a huge spread of retreat rates in response to different combinations of flux gate width, ice thickness and water depth (Enderlin and others, 2013; Åkesson and others, 2018; Frank and others, 2022). Lessons learned from studies on ice-sheet outlet glaciers underline these findings (e.g. Nick and others, 2013; Catania and others, 2018; Choi and others, 2018).

We hypothesize that in most future projections, the underestimation of ice thickness towards tidewater glacier fronts creates a time lag in the response of these glaciers to external forcing and thus a considerable uncertainty regarding the trajectories of sea level-relevant mass losses. This issue may have severe consequences for the accuracy and reliability of calculations of mass losses from tidewater glaciers around the world. We expect the time lag to primarily develop during the early years of the projection period when mass loss by calving flux is presumably underestimated because of limited flux gate cross-sectional sizes. In addition, we expect retreat rates during this period to be underestimated because of limited water depths, which prohibit faster retreats of a tidewater glacier tongue in a flotation model environment.

The aim of this paper is to present a sensitivity study that analyses and quantifies the variability in timing and amount of modelled future sea level-relevant mass losses from a tidewater glacier with respect to different bedrock topographies and flotation characteristics. While in general the sensitivity of tidewater

glacier retreat and mass loss to bedrock topography is well-known (e.g. Hanson and Hooke, 2000; Oerlemans and others, 2011), a comparison of a variety of readily available, modelled bedrock datasets as they are frequently employed in global-scale glacier projections (Hock and others, 2019) has not been performed yet. Our sensitivity study is carried out exemplarily for the well-studied tidewater glacier Hansbreen in southern Svalbard (Fig. 1). We calculate sea level-relevant mass losses from the glacier due to climatic mass balance (CMB), calving flux and calving front retreat, as well as the resulting changes to the 3-D glacier ice body by using a simple, evolution-oriented, non-dynamic glacier model. Our sensitivity study accounts for variability in external forcing by considering different prescribed mass-balance regimes.

We do not intend to project actual glacier changes. We rather present a conceptual modelling study that is able to capture a theoretical range of potential glacier responses to a comprehensive variety of framework conditions and forcing scenarios. Hereby, the latter plays a dual role: the different forcing scenarios are not only intended to represent different settings of the glacier, but are also used to assess potential impacts of different future climate change scenarios. In the end, we concentrate on constraining potential mass-loss trajectories of the glacier while especially focusing on the identification of differences between the different bedrocks.

Study area

Hansbreen is a tidewater glacier draining into Hansbukta, a small bay at the northern coast of the Hornsund fjord, southern Spitsbergen, Svalbard (Fig. 1). The glacier is polythermal (Jania and others, 1996) and has an overall extent of $\sim 54 \text{ km}^2$ (Błaszczuk and others, 2013). It is situated in a region that is characterized by almost continuously negative CMBs since the beginning of the 20th century (Möller and Kohler, 2018), and by a regional equilibrium line altitude (ELA) of $\sim 390 \text{ m a.s.l.}$ in 2000–11 (Möller and others, 2016b). The majority of glacierized areas in this region lies still above the ELA, but albedo data revealed that, over recent decades, glacier surfaces in southern Spitsbergen have experienced one of the strongest changes across the entire Svalbard archipelago (Möller and Möller, 2017). Differing from the regional mean, Hansbreen, which spans an altitude range from above 700 m a.s.l. down to sea level, has a mean elevation of $\sim 290 \text{ m a.s.l.}$ (Błaszczuk and others, 2013) and is thus largely (77%) situated below the regional ELA.

In the beginning of the 20th century Hansbreen extended further across Hansbukta filling it out entirely (Błaszczuk and others, 2013). Since then, the glacier retreated at highly varying annual rates with the most present retreat rates being $\sim 40 \text{ m a}^{-1}$ (Vieli and others, 2002; Błaszczuk and others, 2009; Ćwiąkała and others, 2018). The calving front has a length of $\sim 1.5 \text{ km}$ and a thickness of $\sim 100 \text{ m}$ at the central flowline of the glacier, where water depth is $\sim 55 \text{ m}$, as determined by a combination of ground-penetrating radar and bathymetric measurements (Otero and others, 2017). As shown by ground-penetrating radar data, the maximum ice thickness of Hansbreen is $\sim 400 \text{ m}$, the underlying bedrock is reverse-sloping over the first $\sim 4 \text{ km}$ from the terminus with below sea level elevations extending over more than two-thirds of the glacier along the central flowline (Grabiec and others, 2012). Water depths in Hansbukta in the forefront of the glacier reach down to more than 80 m (Ćwiąkała and others, 2018; De Andrés and others, 2018, 2021).

Data

For our study we rely on different sources of topographic data for the 3-D ice body of Hansbreen. We use four modelled ice thickness

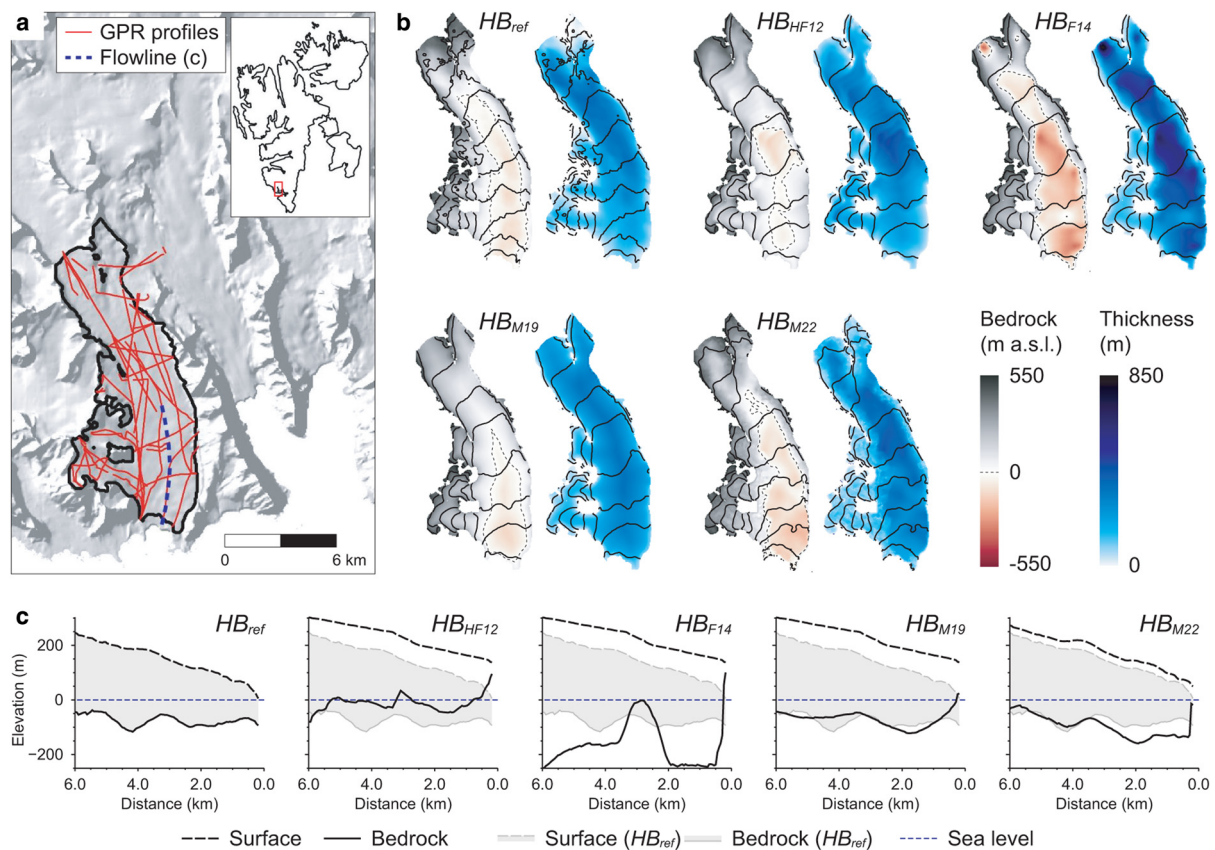


Fig. 1. Overview of the greater study area (a) and of the five different 3-D ice bodies of Hansbreen that are compared in this study (b). The location of Hansbreen is indicated in (a) by the black glacier outline. Profiles of the ground-penetrating radar (GPR) profiles used to create the reference 3-D ice body (ref in (b) and (c)) are shown as red lines. The background shading in (a) is derived from the DEM *Terrengmodell Svalbard (S0 Terrengmodell)* (Norwegian Polar Institute, 2014). For each of the five different 3-D ice bodies of Hansbreen, bedrock topography and ice thickness are shown as maps (b), and flowline profiles (c). Each map also shows the respective surface topography as contours with a spacing of 50 m. The five 3-D ice bodies are the reference ice body which is based on ground-penetrating radar measurements (ref) and four modelled bedrock datasets which are taken from Huss and Farinotti (2012) (H12), Frey and others (2014) (F14), Maussion and others (2018) (M18) and Millan and others (2022) (M22).

datasets and an ice thickness distribution based on direct measurements which represents the reference. In combination with specified surface topography datasets, the ice thicknesses allow for the calculation of associated bedrock topography datasets.

The reference consists of a bedrock topography dataset ($h_{b,ref}$; Figs 1b, c) that is derived from extensive measurements along ground-penetrating radar profiles (Fig. 1a) and subsequent geostatistical inter/extrapolation (Grabiec and others, 2012; Navarro and others, 2014) and a surface topography ($h_{s,ref}$) taken from the DEM *Terrengmodell Svalbard (S0 Terrengmodell)* provided by the Norwegian Polar Institute (2014).

Three modelled bedrock topography datasets are derived from data of the Ice Thickness Models Intercomparison eXperiment (ITMIX; Farinotti and others, 2019). Within ITMIX, four different ice thickness models cover the Svalbard archipelago. However, we omit the model by Fürst and others (2018) as it ingests the rich set of ice-thickness data available for Hansbreen and thus created a bedrock topography that is very similar to our reference dataset. All three models use the same surface topography dataset ($h_{s,1}$) as input, i.e. Arctic DEM version 2 (Porter and others, 2018). Named after the respective ice thickness models, we calculate the bedrock topography datasets $h_{b,HF12}$ (Huss and Farinotti, 2012), $h_{b,F14}$ (Frey and others, 2014) and $h_{b,M19}$ (Maussion and others, 2019). These three datasets all show the initially described underestimation of ice thickness towards the calving front (Fig. 1c), despite their different treatments of near-terminus mass fluxes. Huss and Farinotti (2012) account for a potential flux at the terminus in a very general way, which is not imposed and verified for

individual glaciers. Frey and others (2014) derive ice thickness based on local surface slope only. In their method, the flux is irrelevant and therefore also the condition of zero flux at the terminus as imposed by other ice thickness models. Maussion and others (2019) do not account at all for any mass flux at the terminus in their bed inversion. Further comparative information about the different models can be found in Farinotti and others (2019).

The fourth modelled bedrock topography dataset (Figs 1b, c) is derived from the study of Millan and others (2022). Based on a surface topography that combines Arctic DEM and TanDEM-X elevations ($h_{s,2}$) and extensive, remotely sensed surface ice flow velocity data, this study delivers modelled ice thicknesses that do not suffer from a tendency to an underestimation of close-to-terminus ice thickness (Fig. 1c). Based on these data sources we calculate the bedrock topography dataset $h_{b,M22}$ (Millan and others, 2022).

All datasets are reprojected to Universal Transverse Mercator zone 33N and resampled to a uniform 50 m resolution. The outlines of Hansbreen are taken from the *Randolph Glacier Inventory (RGI) 6.0* (Pfeffer and others, 2014). From these data we create five different 3-D ice bodies of Hansbreen which correspond to considerably different sea level-relevant ice volumes (Table 1; Fig. 1).

We further use measured surface mass-balance data from a set of 11 stakes on Hansbreen, which are distributed between 60 and 500 m a.s.l. and cover the period 2000–11 for defining present-day mass-balance distribution (Möller and others, 2016b).

Table 1. Overview of the five different 3-D ice bodies of Hansbreen, that are created by combining the given surface and bedrock elevation datasets

ID	Surface elevation	Bedrock elevation	Ice volumeGt
HB_{ref}	$h_{s,ref}$ Terrengmodell Svalbard (S0 Terrengmodell) (Norwegian Polar Institute, 2014)	$h_{b,ref}$ (Grabiec and others, 2012; Navarro and others, 2014)	8.8
HB_{HF12}	$h_{s,1}$ Arctic DEM (Porter and others, 2018)	$h_{b,HF12}$ (Huss and Farinotti, 2012)	10.7
HB_{F14}	$h_{s,1}$ Arctic DEM (Porter and others, 2018)	$h_{b,F14}$ (Frey and others, 2014)	11.2
HB_{M19}	$h_{s,1}$ Arctic DEM (Porter and others, 2018)	$h_{b,M19}$ (Mausson and others, 2019)	11.0
HB_{M22}	$h_{s,2}$ Arctic DEM and TanDEM-X (Millan and others, 2022)	$h_{b,M22}$ (Millan and others, 2022)	9.3

The IDs (HB_x) and bedrock elevation datasets ($h_{b,x}$) of all 3-D ice bodies (except for the reference ice body) are named after the study that presented the modelled ice thickness dataset used to calculate bedrock elevations. References for the different datasets are given in parentheses. The sea level-relevant ice volumes of each 3-D ice body are given in addition. HB_{HF12} , HB_{F14} and HB_{M19} are taken from ITMIX (Farinotti and others, 2019).

Methods

In our sensitivity study we compare the projected sea level-relevant mass losses from the five different 3-D ice bodies of Hansbreen. We use a simple, evolution-oriented tidewater glacier model, which is by purpose limited to a straightforward from-forcing-to-outcome design. It does not resolve ice flow, but is based on mass conservation principles instead. The model is forced by prescribed, idealized annual CMB profiles (i.e. specifications of CMB as functions of altitude (Cogley and others, 2011)) and annual calving rates that are calculated from water depth-dependent ice flow velocities. In the model, we apply a range of empirical parameters that makes the marine-terminating tongue of the glacier evolve either grounded or floating. We carry out five experiments with different, prescribed CMB profiles referring to different climate settings (cf. subsection 'Climate experiments'). The model delivers sea level-relevant mass loss from CMB, calving flux and calving front retreat. This means it separately calculates mass changes above and below sea level and accounts for changes in displaced sea water. For simplicity, we only use the terms mass loss or mass change in the following. Modelling is done in annual time steps over a 500 year period on a 50 m resolution grid.

Model description

The model is based on an extended version of the glacier topography feedback approach of Huss and others (2008), which has been successfully applied in glacier evolution modelling on Svalbard before (Möller and others, 2016a), in combination with the flotation criterion-based calving model of Vieli and others (2002). It calculates mass changes due to annual CMB and calving flux in a non-dynamic way (i.e. not resolving ice flow). The adjustment of the glacier ice body assumes an instantaneous response to these annual mass changes and involves two consecutive procedures: (1) changes of the surface elevations of the ice body and (2) changes of the extent of the ice body. Surface elevation changes occur as direct response to CMB-related mass gains in the accumulation area, CMB-related mass losses in the ablation area and calving flux-related mass losses at the glacier front. Changes to the glacier's extent occur as indirect response to decreasing ice thickness, which results from surface elevation changes, by applying the flotation criterion. Figure 2 shows an overview of the workflow within the model.

Each annual modelling time step starts with an extrapolation of the prescribed CMB profile over the transient glacier surface topography. This facilitates a continuous feedback between CMB and surface elevation which is crucial to avoid considerable misestimations of future mass losses (Schäfer and others, 2015).

The CMB-related mass loss is then calculated by integrating the annual CMB field over the grounded part of the glacier. Mass loss from floating parts of the glacier is not considered, as it is not sea level-relevant. Parallel to this and as long as the glacier is marine-terminating, the calving flux-related mass loss is calculated by multiplying the transient cross section of the flux gate by the ice flow velocity. The size of the flux gate is calculated as the integral over transient ice thickness along the ice-water boundary at the glacier front, while ice flow velocity (v) is calculated from mean water depth (d_w) along this boundary according to:

$$v = 30 + 1.54d_w \quad (1)$$

This empirically based relationship scales the ice flow velocity between 110 m a^{-1} for a water depth of 52 m and 30 m a^{-1} for a water depth of 0 m, when the glacier becomes land-terminating and calving-flux stops. The velocity of 110 m a^{-1} represents a simplified mean over various measurements at Hansbreen in recent decades (Vieli and others, 2000, 2002; Otero and others, 2017), while the water depth of 52 m represents initial conditions according to $h_{b,ref}$ averaged along the glacier front. Water depth-dependent calving flux is a well-established, albeit simplifying, parameterization method (e.g. Pelto and Warren, 1991), that fits to the intended simplicity of our model.

The following adjustment of glacier surface elevations (procedure A, Fig. 2) varies in parts according to the sign of glacier-wide CMB. In case of a negative glacier-wide CMB, the adjustment of surface elevations to CMB-related mass losses (sub-procedure A₁) is limited to the ablation area only: surface elevations in the ablation area are first uniformly increased by the specific (positive) CMB of the accumulation area and then decreased according to the spatially distributed (negative) CMB field of the ablation area. This results in an unintentional increase of surface elevations in the vicinity to the equilibrium line. The latter is corrected for by distributing the integrated volume of this increase down-glacier to gradually revoke surface elevation decreases gridcell by gridcell until none of the excess volume is left. Thus, the area of unchanged surface elevations finally extends beyond the lower border of the accumulation area and into the ablation area. In case of a positive glacier-wide CMB, surface elevations across the entire glacier are uniformly increased by the glacier-wide specific (positive) CMB. This mimics a redistribution of upper-glacier mass gains by glacier dynamics. Finally, the glacier ice body is adjusted to calving flux-related mass losses (sub-procedure A₂) by assuming homogeneous dynamical thinning: surface elevations across the entire glacier are uniformly decreased until the resulting integrated volume of the glacier-wide mass loss equals the volume of the calving flux. This implies an unchanged

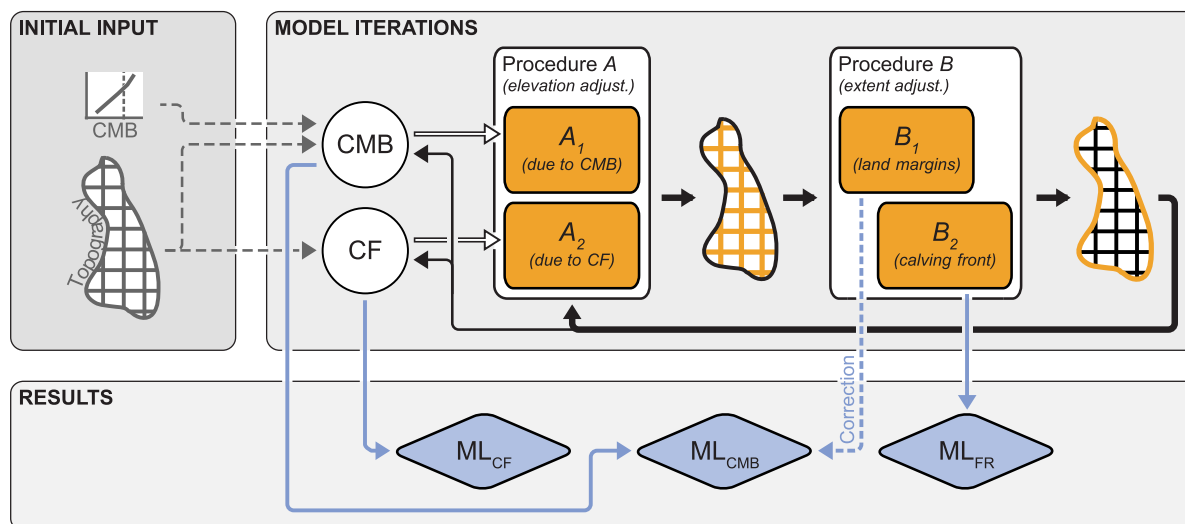


Fig. 2. Workflow of the glacier model. The initial input consists of a 3-D ice body of Hansbreen (surface and bedrock grids) and of prescribed CMB profiles (cf. Table 2). Annual modelling time steps start with calculations of glacier-wide CMB and calving flux (CF). Dashed grey, thin black and black/white arrows indicate input to the model's calculations and adjustment procedures. Thick black arrows indicate evolution of the 3-D ice body. Adjustment procedure A changes the surface topography of the glacier (indicated by orange hashing), while adjustment procedure B changes its extent (indicated as orange line). Blue arrows indicate model output in form of mass loss resulting from either calving flux (ML_{CF}), climatic mass balance (ML_{CMB}) or frontal retreat (ML_{FR}).

ice body in case of a positive glacier-wide CMB and the occurring calving flux compensating for each other. During model runs with a floating glacier front, the adjustments of the ice body by decreasing surface elevations and ice thicknesses imply an imbalance of buoyancy forces across the floating part of the tongue. To correct for this physical inconsistency, surface elevations of the affected gridcells are increased until balance is restored, while ice thickness remains unchanged. The model hereby assumes densities of 1030 kg m⁻³ for sea water and 900 kg m⁻³ for glacier ice.

The adjustment of glacier extent (procedure B, Fig. 2) varies between the land-terminating margins (sub-procedure B₁) and the calving front (sub-procedure B₂) of the glacier and responds to the previous changes in surface elevation. Along the land-terminating glacier margins, the model identifies and removes gridcells where the lowering of the glacier surface in procedure A creates negative ice thicknesses. A similar reduction of glacier extent may also occur across pronounced rises in the bedrock topography, where ice thicknesses are small. Hence, nunataks in the glacier ice body may also develop. The annual mass loss by glacier-wide CMB, which is calculated at the beginning of each annual modelling time step, is corrected accordingly.

Along the calving front, the model identifies and removes gridcells where the lowering of the glacier surface in procedure A makes ice thickness drop below a certain threshold, that is related to flotation thickness. This parameterization mimics increasing buoyancy forces that lead to unstable conditions in the glacier tongue and subsequent calving. The threshold ice thickness (\hat{t}_i) is calculated according to Vieli and others (2002) as a function of water depth (d_w) and the density ratio between sea water ($\rho_w = 1030 \text{ kg m}^{-3}$) and glacier ice ($\rho_i = 900 \text{ kg m}^{-3}$):

$$\hat{t}_i = \beta \frac{\rho_w}{\rho_i} d_w \quad (2)$$

The flotation parameter β is varied between 0.6 and 1.4 (in steps of 0.05, yielding 17 different flotation parameter values) in order to simulate different buoyancy conditions across the marine-terminating glacier tongue. Special attention is paid to $\beta = 1.15$, which has been found to most closely resemble real conditions at Hansbreen (Vieli and others, 2002). $\beta \geq 1$ implies a grounded and $\beta < 1$ a floating tongue. Hence, the smaller β the thinner the

tongue may become before ice break-up occurs and the glacier extent is reduced. The model limits this reduction to directly water-neighbouring gridcells in order to ensure that calving front break-up only happens as a contiguous frontal retreat. At the end of each model iteration, mass loss from calving front retreat is calculated in case of grounded ice. Mass loss from a floating tongue is not considered, as it is not sea level-relevant.

Climate experiments

We carry out five individual experiments to simulate different climate settings for Hansbreen. Each experiment is defined by a specific CMB profile and, in two cases, its variability with time (Table 2). Our control experiment (Ex_0) is defined by an in situ-measured profile. This profile is created as a linear fit (function of elevation) to a total of 110 annual measurements at 11 mass-balance stakes on Hansbreen in the period 2000–11 (Möller and others, 2016b). It remains constant over the 500 year modelling period.

The other four experiments (Table 2) are designed to represent alternative, time-invariant climate settings ($Ex_{1a,b}$) and linearly changing climates ($Ex_{2a,b}$). All four are defined on the basis of the in situ-measured profile of Ex_0 . $Ex_{1a,b}$ are meant to represent warmer climates at two different intensities. For these experiments the profile is shifted towards more negative balances, with shifts being stronger for the ablation area than for the accumulation area. The shifted profiles are meant to represent Representative Concentration Pathway (CP) 4.5 and RCP 8.5 conditions in the middle of the 21st century. They are defined according to the mean projected CMB profile at the adjacent Werenskiöldbreen for the period 2048–52 that has been simulated based on a distributed model (Möller and others, 2016a). The RCP 4.5 profiles roughly match those presented by van Pelt and others (2021) for southern Svalbard in general. $Ex_{2a,b}$ are meant to represent continuously warming climates at two different rates. The profiles in these experiments are linearly changing over the modelling period. Starting from Ex_0 they reach the step shifts of $Ex_{1a,b}$ after 50 years.

The implementation of the five experiments in our sensitivity study is complicated by the fact that the five 3-D ice bodies of Hansbreen that we compare are co-defined by three different

Table 2. Definitions of annual CMB profiles of the five experiments

Experiment	CMB ₀ m w.e.	Gradient m w.e. m ⁻¹
<i>Ex</i> ₀	-1.94	+0.0053
<i>Ex</i> _{1a}	-4.57	+0.0077
<i>Ex</i> _{1b}	-8.31	+0.0093
<i>Ex</i> _{2a}	$-1.94 + j \frac{-4.57+1.94}{50}$	$+0.0053 + j \frac{0.0077-0.0053}{50}$
<i>Ex</i> _{2b}	$-1.94 + j \frac{-8.31+1.94}{50}$	$+0.0053 + j \frac{0.0093-0.0053}{50}$

Each profile is defined by the climatic mass balance at sea level (CMB₀) and the elevational gradient. The profile of the control experiment *Ex*₀ is derived from stake measurements on Hansbreen over 2000–11 (Möller and others, 2016b). The profiles of *Ex*₀ and *Ex*_{1a/b} are time invariant. The latter represent RCP 4.5 and RCP 8.5 conditions at the middle of the 21st century. The profiles of *Ex*_{2a/b} vary linearly over the modelling period (with *i* = 0, ..., 500 years), while reaching the profiles of *Ex*_{1a/b} after 50 years.

surface topographies (Fig. 1b). As we intend to study the sensitivity of projected mass losses to bedrock topography only, we have to make sure that the CMB profiles of our experiments provide equal forcing to all of those ice bodies independent of their individual surface topography. In order to facilitate this equal forcing, it is necessary to adjust the CMB profiles of the experiments to the two surface topographies (*h*_{s,1} and *h*_{s,2}) that co-define the four non-reference ice bodies. An adjustment to the surface topography of the reference ice body (*h*_{s,ref}; Fig. 1b) is not necessary, as the locations and elevations of the mass-balance stakes that form the basis of the CMB profiles in our experiments (Möller and others, 2016b) comply with this surface topography. We therefore calculate adjustment functions that transfer the *h*_{s,ref} elevations to the levels of the *h*_{s,1} and *h*_{s,2} elevations by comparing the surface elevations of the three datasets (Fig. 3). These functions are applied to the CMB profiles in the respective model runs.

Results and discussion

Control runs

As a baseline for our analysis, we use a set of control runs. For these runs, the model is applied to the reference 3-D ice body of Hansbreen (*HB*_{ref}; Fig. 1b) and forced by the control experiment (*Ex*₀; Table 2). All 17 values of the flotation parameter β (Eqn (2)) are considered. The control runs show the future evolution of Hansbreen under constant climate conditions and with the best possible bedrock representation in the model. The run featuring β = 1.15 shows the most probable evolution, as flotation

characteristics in the model equal measured conditions in this case (Vieli and others, 2002).

In the control runs, a continuous retreat of *HB*_{ref} occurs over the modelling period (Fig. 4a). *HB*_{ref} vanishes before the end of the study period (500 years) if the glacier tongue is assumed to be grounded (β > 1.0). The retreat starts at the lowermost parts of the glacier and concentrates mostly on the marine-based parts of the ice. It soon unveils a strongly diverse reaction of the marine-terminating tongue, depending on the flotation parameter. As expected, the retreat is much slower in model runs that allow for a floating tongue (β < 1.0). Accordingly, maximum deviations of the β = 1.15 run from runs with higher flotation parameters reach their peak after already 155–162 years, while for deviations from runs with lower flotation parameters this happens only after 168–202 years (Fig. 4a). Afterwards, deviations between the different model runs decrease and considerable deviations continue to exist only for floating-tongue conditions after ~300 years, as the glacier becomes land-terminating under grounded-tongue conditions at this time. For the former (β < 1.0), a complete disappearance of *HB*_{ref} does not occur until the end of the modelling period. The exact timing of its disappearance under grounded-tongue conditions is related to the assumed flotation parameter (Fig. 4a), disappearing later as the flotation parameter decreases.

The retreat pattern over the first 300 years mirrors water depth variations. For a given depth, the ice thickness necessary to preserve a stable tongue increases with the assumed flotation parameter. This means that for increasing water depths and a given ice thickness, the flotation parameter needs to decrease to still assure stability of the tongue. This explains the variation in the observed increases of the retreat rates at the moment when the glacier tongue approaches deeper waters. In model runs with higher flotation parameters, i.e. with grounded tongues, the increase is stronger and occurs earlier than in runs with lower flotation parameters, i.e. with floating tongues.

The retreat pattern is also mirrored in the total mass loss (Fig. 5a). The similarity between the spread of the retreat trajectories of the individual model runs (Fig. 4a) and the spread of the total mass-loss trajectories (Fig. 5a) comes despite the fact that the shares of the three individual processes that contribute to total mass loss (CMB, calving flux and frontal retreat) develop non-uniformly over the modelling period (Fig. 5a). Cumulative mass loss by CMB develops rather independently from the assumed flotation parameter over the first half of the modelling period, with deviations not exceeding ±0.3 Gt (Fig. 5a).

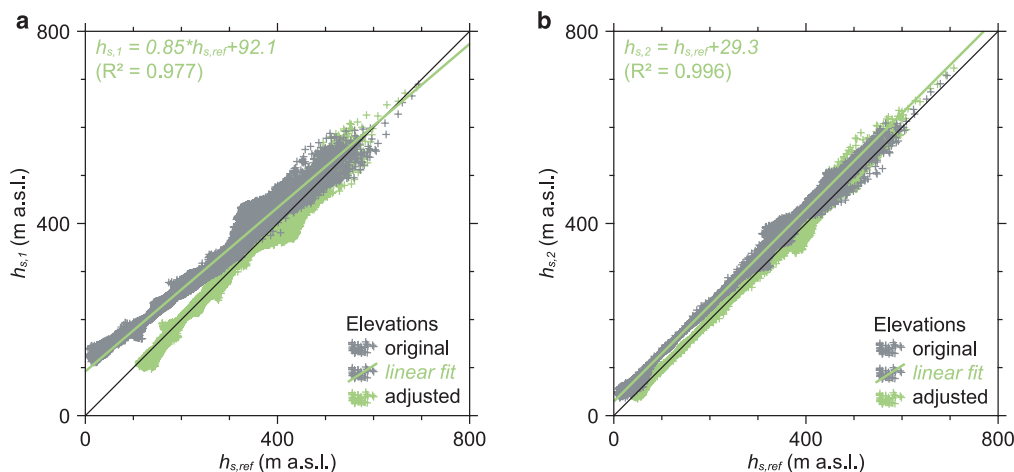


Fig. 3. Comparisons of the reference surface topography (*h*_{s,ref}) to the levels of surface topographies *h*_{s,1} (a) and *h*_{s,2} (b). Transfer functions from the former to the latter and resulting adjustments (cf. subsection ‘Climate experiments’) are displayed in green.

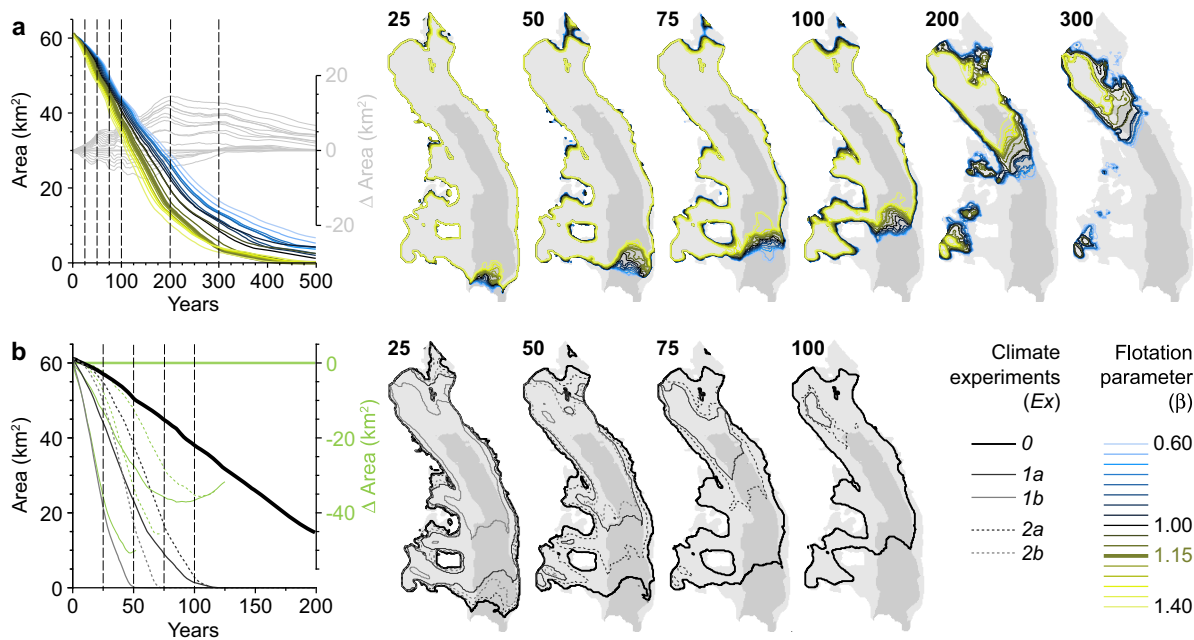


Fig. 4. Modelled area of Hansbreen represented by its reference 3-D ice body (HB_{ref}) over the study period. The control runs (climate experiment Ex_0 with different flotation parameters) are shown in (a) and runs comparing different climate experiments (all with flotation parameter $\beta = 1.15$) are shown in (b). The absolute areal retreats in (a) are shown along with differences to the model run with the observed flotation parameter $\beta = 1.15$ (light grey) and those in (b) are shown along with differences to the model run Ex_0 (light green). Years with areal representations of the glacier extent (right) are indicated by dashed vertical lines in the graphs (left). The year of each set of extents is given at the top right of the glacier. The initial glacier area is marked in grey, with the submerged part of the bedrock indicated in dark grey.

Afterwards, they increase with a decreasing flotation parameter. This is because of a far longer preservation of large parts of the ablation area which lie on the floating part of the glacier tongue. Contrary to this, the rates of mass loss by calving flux differ by factors of up to ~ 2.5 depending on the assumed flotation

parameter (Fig. 5a), as long as the marine-terminating front of the glacier remains in deeper waters (cf. Fig. 1b). The rates become almost independent of the assumed flotation parameter afterwards (Fig. 5a). In general, cumulative mass losses from calving flux increase with an increasing flotation parameter, as the

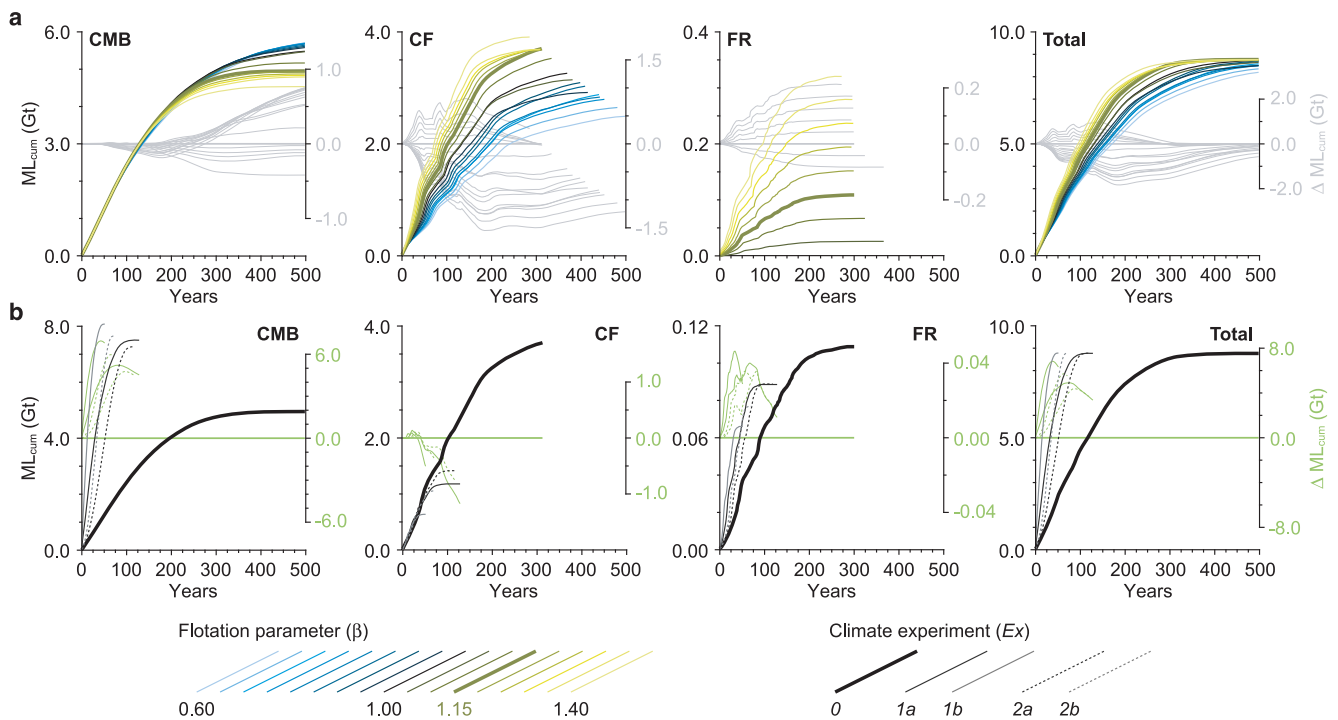


Fig. 5. Cumulative mass losses from Hansbreen represented by its reference 3-D ice body (HB_{ref}) over the study period. Mass losses are shown divided into mass loss due to CMB, calving flux (CF) and calving front retreat (FR). The total mass losses are shown in addition. The control runs (climate experiment Ex_0 with different flotation parameters) are shown in (a) and runs comparing different climate experiments (all with flotation parameter $\beta = 1.15$) are shown in (b). The cumulative mass losses in (a) are shown along with differences to the model run with the observed flotation parameter $\beta = 1.15$ and those in (b) are shown along with differences to the model run Ex_0 .

glacier tongue remains grounded even in deeper waters. This in turn increases ice thickness and thus the cross section of the flux gate. Frontal retreat is of minor importance for total mass loss compared to CMB and calving flux. The cumulative values are one order of magnitude smaller over the entire modelling period, independent of the assumed flotation parameter (Fig. 5a).

Influence of climate

To isolate the influence of different climate forcing, we use a set of model runs that are based on the reference 3-D ice body of Hansbreen (HB_{ref} ; Fig. 1b), but (other than the control runs) are forced by the four alternative experiments $Ex_{1a/b}$ and $Ex_{2a/b}$ (Table 2). In this case, the runs are performed with the observed flotation parameter ($\beta = 1.15$; Eqn (2)) only.

As expected, the retreat of HB_{ref} occurs faster the more negative the applied CMB profiles are (Fig. 4b). When assuming linearly warming climates ($Ex_{2a/b}$) the retreat trajectories increasingly diverge over the modelling period and the life span of the glacier is drastically reduced. For the stronger warming scenario Ex_{2b} , the glacier already disappears after 72 years, which means a reduction of its life-time of at least 85% compared with constant present climate conditions. As Ex_{2b} resembles RCP 8.5 conditions in southern Svalbard over the current century (Möller and others, 2016a), this result impressively illustrates the increasing imbalance with climate of Svalbard glaciers. In the partitioning of mass losses, constantly warming climates lead to a considerable shift from frontal to surface mass loss (Fig. 5b). As the more negative CMB increases surface mass loss, it leads to a stronger thinning of the glacier tongue and thus to an earlier ice break-up at the front. The latter is

illustrated by strongly increased frontal retreat rates in $Ex_{2a/b}$ when compared with Ex_0 (Fig. 5b). The stronger thinning also implies reduced flux gate cross sections and thus considerably reduced calving fluxes.

Influence of bedrock topography

For describing the sensitivity of glacier evolution to the usage of different bedrock topographies in our model to project future glacier evolution we show two sets of analysis: (1) model runs with Ex_0 forcing that consider all 17 flotation parameters β (Fig. 6), and (2) model runs with forcing by all five climate experiments (Table 2) that only consider the observed flotation parameter ($\beta = 1.15$; Fig. 7). This allows us to clearly distinguish between the different influencing factors.

Bedrock elevations play a key role for the characteristics of retreat and mass-loss trajectories. The considerably varying depths and extents of the submarine parts of the different bedrocks (Fig. 1) induce highly variable retreat trajectories (Fig. 8) that develop independent from the trajectories of total mass loss (Figs 6, 7). Surface and frontal mass loss, which together form total mass loss, develop non-uniformly with respect to different bedrock topographies. In all five climate experiments, frontal mass loss differs much more markedly than surface mass loss, and the course of the frontal mass-loss trajectories is even dominant enough to decisively imprint on total mass-loss trajectories (Figs 6, 7). However, under $Ex_{1a/b}$ and $Ex_{2a/b}$ forcing the total mass-loss trajectories increasingly mirror the trajectories of surface mass loss over the years of modelling (Fig. 7). This suggests that in warmer climates mass loss at the glacier front loses both its qualitative importance (for the course of the total

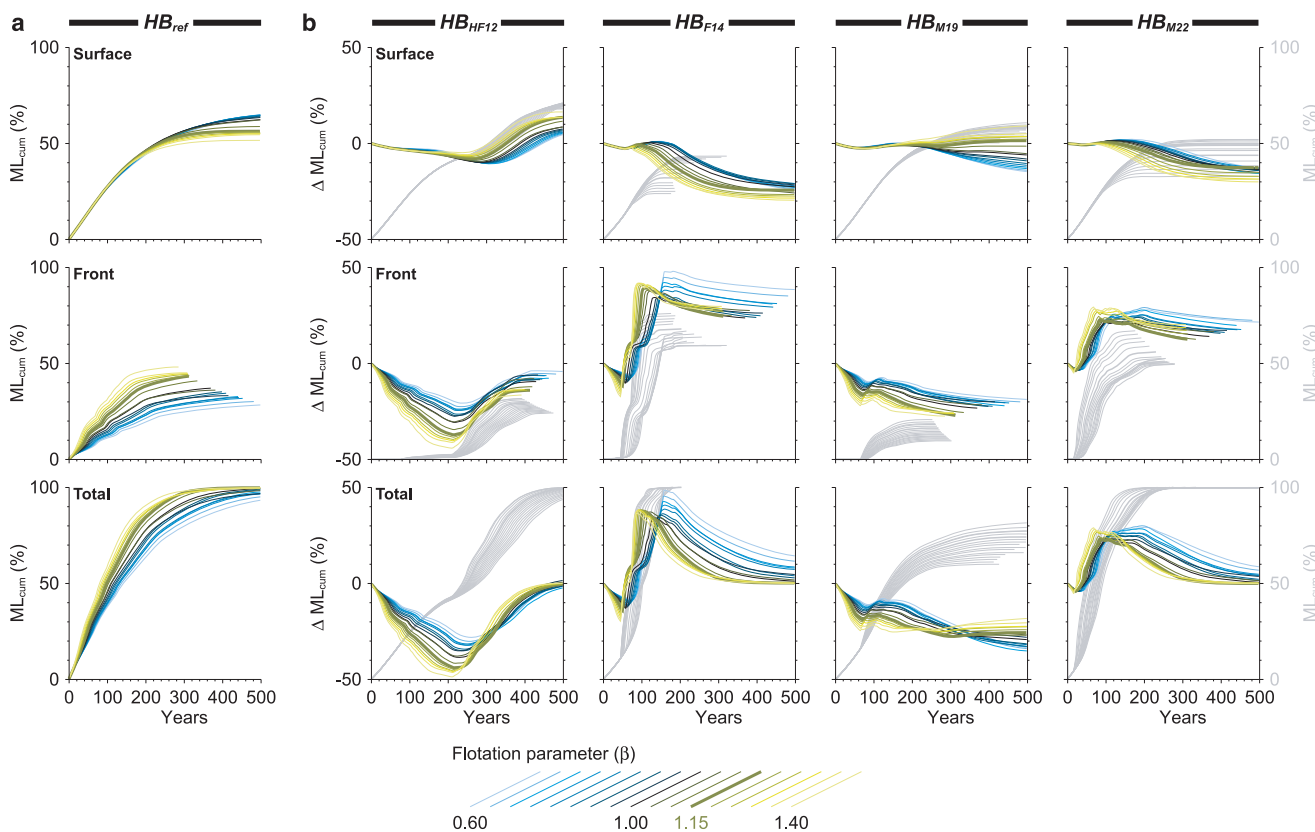


Fig. 6. Comparison of cumulative mass losses from Hansbreen over the study period from the five 3-D ice bodies for different flotation parameters. All model runs are forced by climate experiment Ex_0 . Mass losses are shown divided into surface mass loss and mass loss at the glacier front (calving flux plus calving front retreat). The total mass losses are shown in addition. For the reference ice body (HB_{ref}), the mass losses are shown as shares of the total ice volume (a). For all other 3-D ice bodies (b), the mass losses are shown as shares of the respective total ice volume (light grey). The differences to the respective shares at HB_{ref} (colour-coded) are shown in addition.

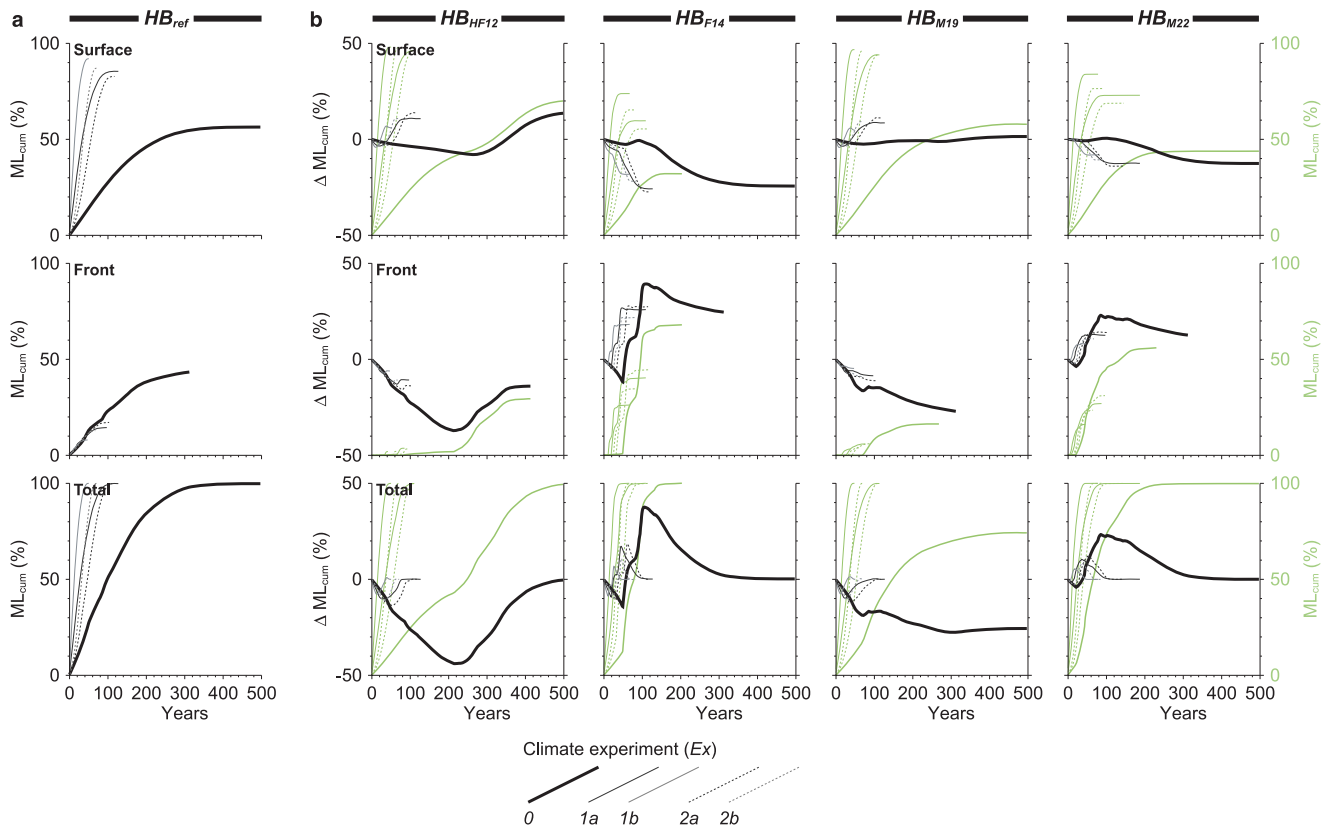


Fig. 7. Comparison of cumulative mass losses from Hansbreen over the study period from the five 3-D ice bodies for the different climate experiments. All model runs are performed with flotation parameter $\beta = 1.15$. Mass losses are shown divided into surface mass loss and mass loss at the glacier front (calving flux plus calving front retreat). The total mass losses are shown in addition. For the reference ice body (HB_{ref}), the mass losses are shown as shares of the total ice volume (a). For all other 3-D ice bodies (b), the mass losses are shown as shares of the respective total ice volume (light green). The differences to the respective shares at HB_{ref} (colour-coded) are shown in addition.

mass-loss trajectory) and also its quantitative importance (with its decreasing share in total mass loss).

When comparing the frontal mass losses from the different 3-D ice bodies in detail, it becomes obvious that over the first couple of decades the contributions from HB_{ref} are generally higher and occur earlier than those from the other four 3-D ice bodies (Fig. 6). This is because of the initially described characteristic underestimation of ice thickness at the glacier front in modelled bedrock datasets (Fig. 1c). The underestimation leads to a time lag in frontal mass loss (Fig. 6b) as the related 3-D ice bodies initially show a land-terminating glacier front. This front needs to retreat due to CMB-related thinning before the submarine part of the bedrock is reached and frontal mass loss via calving flux and calving front retreat can occur. The durations of the time lag reach from 16 years (HB_{M22}) over 45 (HB_{F14}) and 65 years (HB_{M19}) to 75 years (HB_{HF12}) under constant present climate conditions (Fig. 6b) and decrease in warmer climates (Fig. 7), reaching only 14–35 years under Ex_{2b} forcing (Fig. 7b). From these times onwards, the trajectories of cumulative frontal mass loss start to develop according to water depths. Hence, 3-D ice bodies with deeper bedrock troughs (especially HB_{F14} , but also HB_{M22}) strongly overestimate the reference frontal mass loss of HB_{ref} during the later modelling period, while those with shallower bedrocks (HB_{HF12} , but also HB_{M19}) continuously underestimate it (Fig. 6b). The absolute deviations in frontal mass loss between HB_{ref} and the other four 3-D ice bodies are larger for higher flotation parameters during the earlier part of the modelling period (Fig. 6b), as grounded tongues imply larger flux gates and the bedrock-dependent differences in ice thickness are thus more decisive. This pattern reverses as soon as the glacier front leaves the submarine parts of the bed and becomes land-terminating

(Figs 6b, 8). Surface mass losses from the different 3-D ice bodies, in contrast, are almost the same over the first decades of modelling (Figs 6b, 9b), and a dependence on the assumed flotation parameter does not develop until the glacier fronts have retreated towards the central parts of the submarine bed sections (Figs 6b, 8b). The observed patterns of mass loss (Fig. 6b) indicate that the differences of mass loss induced by the use of an inverted bedrock topography are generally larger in the case of a grounded glacier tongue as long as the glacier remains marine-terminating. Under these conditions, the largest difference is, moreover, reached after a shorter amount of time than in the case of a floating glacier tongue. Finally, the share of frontal mass loss in total mass loss increases considerably under grounded-tongue conditions (Fig. 6), and independent from this, it also shows a clear increase with higher depth and volume of the submarine bedrock trough (Fig. 6b). This suggests that, depending on the type of bedrock that is used in a glacier model, an adequate representation of mass-loss processes at the glacier front is of varying relevance for glacier evolution modelling: the thicker the glacier front, the higher is this relevance.

Under alternative, warmer climate forcing, i.e. $Ex_{1a/b}$ and $Ex_{2a/b}$, the described influences of bedrock topography on glacier retreat and mass loss change significantly. These changes not only find expression in a generally shorter life time of Hansbreen for any of the bedrocks considered, but also in generally higher rates of total mass loss (Figs 7, 8). Differences between the five 3-D ice bodies notably occur in the partitioning of total mass loss (Fig. 7b). 3-D ice bodies with deeper bedrocks and higher submarine ice volumes (HB_{F14} and HB_{M22}) overestimate mass loss at the glacier front, but underestimate surface mass loss when compared to HB_{ref} . 3-D ice bodies with shallower bedrocks (HB_{HF12} and HB_{M19}), in contrast, underestimate mass loss at the

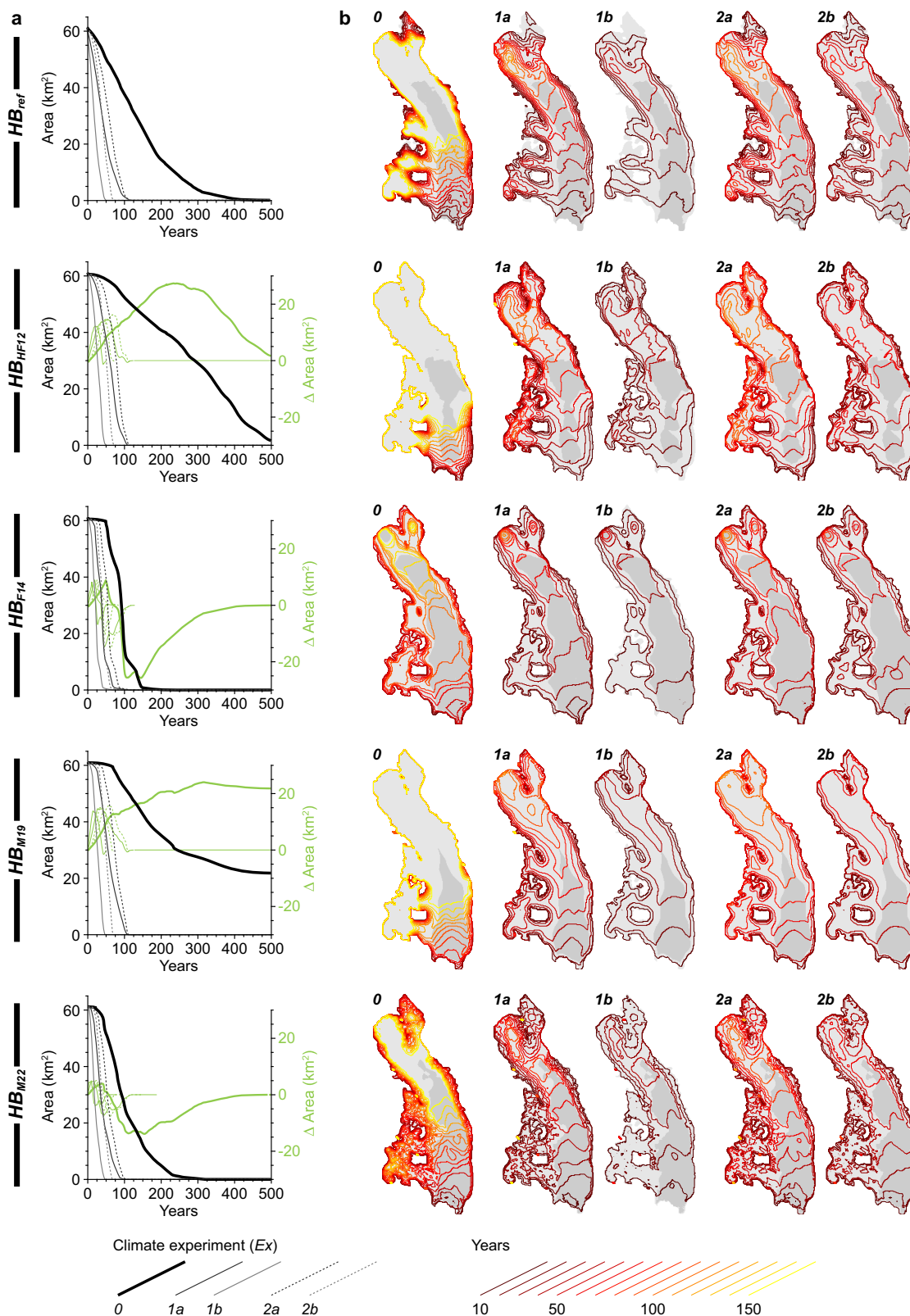


Fig. 8. Comparison of areal retreats of Hansbreen (represented by the five different 3-D ice bodies) over the study period for the different climate experiments. All model runs are performed with flotation parameter $\beta = 1.15$. Areal retreats over time (a) are shown along with maps of time-varying (colour coded) glacier areas (b). In (a), absolute areal retreats (line-style coded) are shown along with differences to the model run Ex_0 (light green).

glacier front, but overestimated surface mass loss. This again supports our previous finding that mass loss at the glacier front becomes more important with increasing frontal thickness. The full influence of climate forcing is, however, more diverse and complex and even alters the sensitivity of the single mass-loss processes to the choice of the flotation parameter (Fig. 9).

For any climate experiment, the spread of cumulative total mass losses after 50 years of modelling in response to different flotation parameters β is by far largest for HB_{F14} . This high sensitivity of HB_{F14} total mass loss to the choice of β is a direct result of the even higher sensitivity of frontal mass loss to β , which is explained by the fact that HB_{F14} has by far the deepest submarine

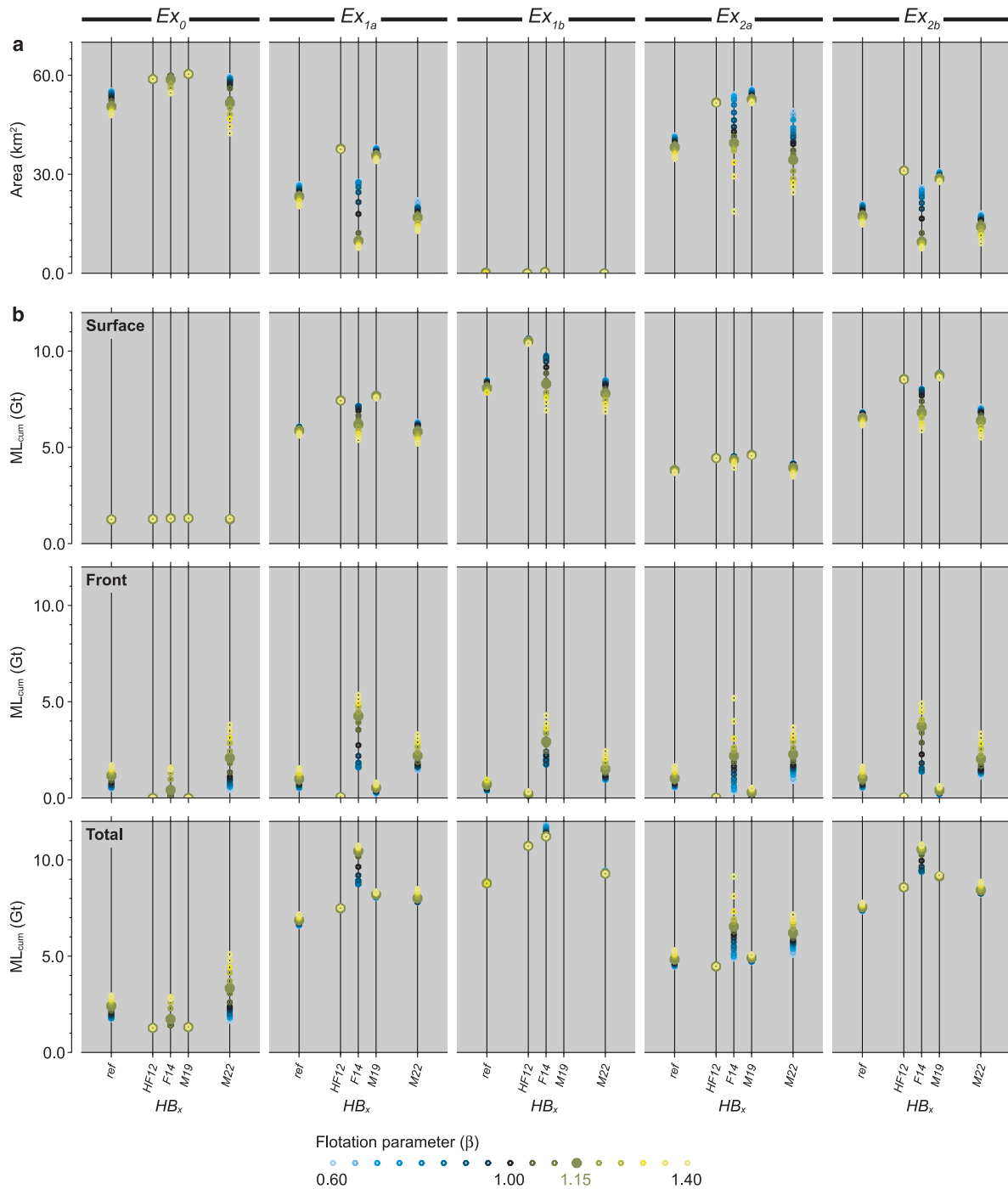


Fig. 9. Comparison of results after 50 years of modelling for the 17 different flotation parameters (colour code), five different 3-D ice bodies (pearl chains in each panel) and five different experiments (columns). Displayed results show the remaining glacier area (a), and the related cumulative mass losses (b): surface mass loss, mass loss at the glacier front (calving flux plus calving front retreat) and total mass loss.

bedrock trough of all five 3-D ice bodies considered in our study. It is, however, noteworthy that the sensitivity of frontal mass loss to β is reduced when applying a warmer climate forcing in the projection model (Fig. 9). This reduction occurs as parts of the sensitivity are moved to surface mass loss, which is directly affected by the more negative CMB of the warmer climates (Fig. 9b). Under Ex_0 forcing, surface mass loss after 50 years hardly shows any sensitivity to β for none of the five 3-D ice bodies. In all other experiments, however, considerable sensitivity is evident. As the increases in sensitivity in surface mass loss more than outweigh the limited changes in sensitivity in frontal mass loss, the resulting total mass loss approaches a zero-sensitivity to β for the warmest climate forcing Ex_{1b} for all 3-D

ice bodies but HB_{F14} (Fig. 9b). These findings imply that the warmer the climate, the more important becomes a reliable knowledge about flotation characteristics of the glacier for projecting surface mass loss. It is striking that such a pattern does not exist for frontal mass loss, even if the latter is directly influenced by the choice of β . Overall, the described effect of warmer climates is amplified for 3-D ice bodies with deeper bedrocks, i.e. HB_{F14} and HB_{M22} .

Under present-climate forcing (Ex_0), HB_{ref} and HB_{M19} show the most similar mass-loss trajectories, as the HB_{M19} bedrock is closest to the reference bedrock of HB_{ref} . Mean differences between the two are smallest over the modelling period and the two show the smallest sensitivities to the choice of β (Fig. 6).

Under Ex_{2b} forcing, the picture becomes different, and the optimal modelled 3-D ice body is HB_{M22} (Figs 7, 10). As this Ex_{2b} experiment represents relatively likely future climate conditions in southern Svalbard (gradual warming over the modelling period according to RCP 8.5), it deserves special attention when discussing the transferability of our results into real-world conditions.

Under Ex_{2b} forcing, the retreat of all four modelled 3-D ice bodies is almost uniformly slower as that of HB_{ref} over the first 14 years of modelling (Fig. 10b). Afterwards, areal retreats of the modelled 3-D ice bodies diverge in relation to water depth at the glacier front (Fig. 10c). Similar to previous observations, the two deeper modelled bedrocks (HB_{F14} and HB_{M22}) show a different evolution pattern than the two shallower ones (HB_{HF12} and HB_{M19}). The bedrock of HB_{M22} is first to allow for a submarine-based glacier front after 11 years and it decreases below the level of the bedrock of HB_{ref} after 15 years. At this time, rates of the differences in areal retreat slowdown markedly (Fig. 10b) and the initial underestimation of cumulative total mass loss starts to decrease towards zero (Fig. 10a). When the retreating front of HB_{M22} reaches the deepest point of the bedrock after 23 years (Fig. 10c), cumulative total mass loss starts to exceed that of HB_{ref} (Fig. 10a) and the areal retreat rate increases considerably (Fig. 10b). In the following years, cumulative mass loss from HB_{M22} is continuously overestimated until the glacier front leaves

the submarine part of the bedrock. A comparable pattern is also observable for HB_{F14} , albeit with higher amplitudes in mass loss and areal extent differences and a later onset of the initial deviation (Figs 10a, b). HB_{HF12} and HB_{M19} , in contrast, do not change between over- and underestimations during their retreat (Figs 10a, b). Cumulative mass loss is continuously underestimated, while the remaining glacier area is always larger than that of HB_{ref} with the respective peak differences occurring during the short period when bedrock elevations decrease below those of HB_{ref} (Fig. 10c).

The existence of these two clearly distinguishable patterns suggests a general principle for glacier evolution modelling in warming climates: glaciers represented by modelled bedrocks all share an initial underestimation of cumulative mass loss. This trend soon changes to an overestimation of cumulative mass loss in case the modelled bedrocks show deeper troughs with high volumes of submarine ice.

Model uncertainty and generalizations

Our results represent the outcome of a conceptual modelling study that is done for the example of a single-test glacier. The employed model considers artificial forcing by prescribed CMB scenarios. A validation of model results and an assessment of model performance can thus not be carried out. However, one of the control runs ($\beta = 1.15$) is designed to closely resemble recent conditions at the glacier. This run results in a retreat of the glacier front of ~ 2.3 – 2.7 km over the first 50 years of modelling. The glacier length record of Hansbreen suggests a retreat of ~ 0.4 – 0.5 km over the first decade of the 21st century (Oerlemans and others, 2011), equalling ~ 2.0 – 2.5 km when extrapolated to a future 50 year period. While our model results account for the positive feedback which exists between glacier thinning and retreat, this effect is not accounted for in the extrapolation of the observation-based retreat. This suggests an underestimation of glacier retreat by the extrapolation and thus a reasonable performance of our model. This is also supported by a future projection of Hansbreen done by Oerlemans and others (2011) which yielded a retreat of ~ 4 km over the period 2000–2100. The model setup used in this study can be seen as a simulated continuation of historic glacier behaviour. Our control runs likewise mimic an unchanged continuation of recent glacier behaviour and suggest a comparable retreat of ~ 3.7 – 4.2 km over the first 100 years of modelling.

When thinking beyond our case study we have to acknowledge that our limited focus on one single-test glacier per se hampers the transferability of the obtained results. Any potential influences of alternative glacier sizes and shapes on the results remain beyond the explanatory power of this study, as do influences of changing glacier dynamics. The design of our model prevents taking into account influences of CMB-induced meltwater availability on ice flow velocity (e.g. Zwally and others, 2002). It also prevents that potential variations of ice flow velocity in response to varying ice discharge or dynamically induced changes in ice mass distribution along the glacier (e.g. Möller and others, 2022) feed back into the modelling chain. Measurements by Vieli and others (2002) suggest that a grounded glacier tongue that approaches flotation thickness during its retreat might experience a short-term increase of flow velocity. Our model does also not account for the known variability of frontal ablation rates with sea-water temperature at Hansbreen (Pętllicki and others, 2015). The introduced uncertainty in the trajectories of projected mass losses has to be borne in mind when transferring our results into generalized statements.

However, and despite these limitations, it is reasonable to expect a more general transferability of our findings. With respect

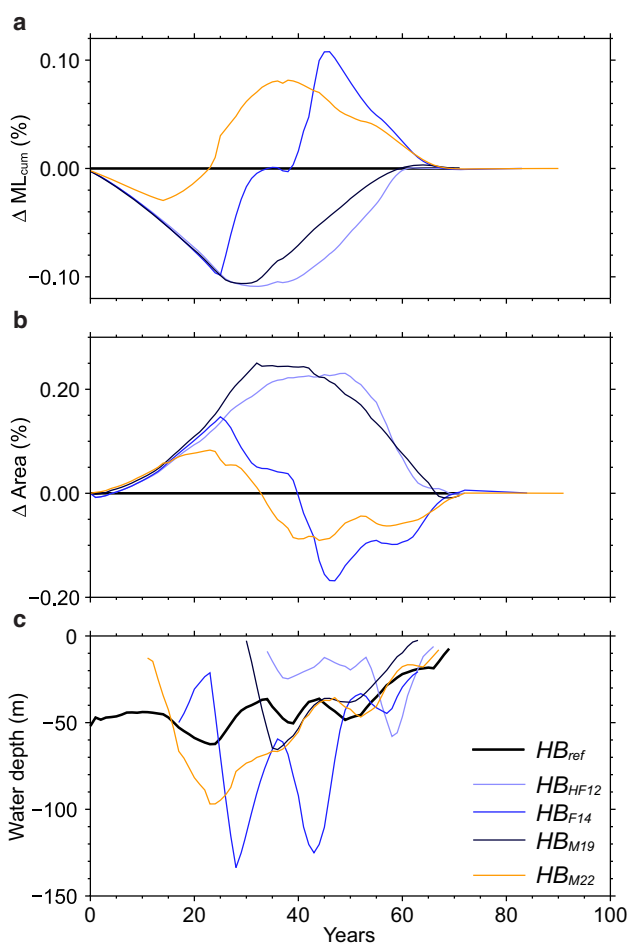


Fig. 10. Cumulative total mass loss (a), glacier area (b) and mean water depth along the glacier front (c) in experiment Ex_{2b} for the five different 3-D ice bodies. (a) and (b) are shown as differences between the shares of the respective total ice volume and glacier area of HB_{ref} and the respective 3-D ice body. Mass loss and glacier area are drawn as long as the respective 3-D ice body continues to exist. Positive mass-loss differences indicate higher cumulative mass loss as HB_{ref} and positive slopes indicate higher mass-loss rates. Negative area differences indicate faster retreat as HB_{ref} and negative slopes indicate higher retreat rates. Water depths are shown as absolute numbers and are drawn only while the respective 3-D ice body is marine-terminating.

to the topographic setting, two main types of tidewater glaciers are commonly found. The glacier bed either transitions rather continuously from above to below zero elevations or it shows an overdeepening close to the glacier's terminus like in the case of Hansbreen. In the latter case, the tidewater glacier terminates on a retrograde-sloping part of the glacier bed, which implies a positive feedback during glacier retreat: the increasing water depth leads to increasing buoyancy forces which in turn lead to faster retreat (e.g. Oerlemans and Nick, 2005; Schoof, 2007). This suggests that tidewater glaciers with qualitatively similar settings to Hansbreen might experience comparable retreat dynamics. The similarity of the topographic setting of these glaciers also implies that modelled bedrock datasets for such glaciers will likely experience similar shortcomings as those that we described for Hansbreen. Hence, we expect the general findings that we obtained in our case study to be qualitatively representative for an entire set of tidewater glaciers. Further studies are nevertheless needed to answer the question of to what extent these findings are also representative for larger and faster tidewater glaciers, where deeper waters might lead to an even more accentuated sensitivity of the retreat dynamics to calving while the glacier front passes the overdeepening. It is left to studies with more sophisticated ice flow models to respond to these and other related questions which cannot be answered here using our simplified glacier model.

Overall, our results suggest that the partitioning of mass loss into the three different processes that are resolved by our approach (CMB, calving flux and frontal retreat) may be highly variable. In the control run, which features a slightly negative CMB, mass losses due to CMB and calving flux are far more important than mass loss due to frontal retreat (Fig. 5). Nevertheless, frontal retreat controls the trajectory of glacier thickness which is mainly governed by bedrock topography. It thus exhibits a major, albeit indirect, control on mass loss by calving flux. This underlines the general importance of accurate bedrock estimates.

From our experiments it becomes obvious that the differences between the trajectories of cumulative total mass loss of HB_{ref} and the four modelled 3-D ice bodies predominantly decrease under warmer climate forcing, i.e. increasingly negative CMB (Fig. 7). When generalizing this effect, it is counteracted by influences of the flotation characteristics. If a glacier is located in colder climates it is more likely to exhibit a floating tongue (van der Veen, 2002). Vaughan and Doake (1996) identified the -5°C mean annual isotherm as a stability threshold for ice shelves and floating tongues on the Antarctic Peninsula. And if such a floating tongue is preserved, the differences between the trajectories of cumulative mass loss of HB_{ref} and the four modelled 3-D ice bodies decrease compared to grounded tongues (Fig. 6). Hence, the influences of the flotation characteristics can be expected to lead to an increase of the differences between the trajectories in warmer climates. This suggests that, depending on which of the two effects described above is larger, the usage of an accurate bedrock and the choice of the right flotation parameter will even become more important in warmer climates, which is of particular relevance in the light of global climate change.

Overall, our results do not allow for a universally valid suggestion regarding the optimal bedrock dataset for projections of future mass loss. For this purpose, results from Ex_{2b} are especially relevant as these experiments feature a gradually warming climate over the modelling period which resembles the RCP 8.5 scenario. For the related projections HB_{M22} seems to be first choice, as both its retreat and its cumulative total mass loss show the smallest mean differences to those of HB_{ref} over the modelling period (Figs 9b, 10a). The maximum underestimation of cumulative total mass loss from HB_{M22} at the beginning of the modelling period is limited to 2.9% (0.2 Gt), while it ranges up to 10% for the

other three modelled 3-D ice bodies (Fig. 10). The related, absolute under- and overestimations of the glacier area over the modelling period are limited to <10% for HB_{M22} , while reaching up to 17% (HB_{F14}), 22% (HB_{HF12}) or even 25% (HB_{M19}). For projections representing the RCP 4.5 scenario, i.e. a slower warming than in RCP 8.5, HB_{M19} performs best, closely followed by HB_{HF12} (Fig. 9b). However, this only applies to cumulative total mass loss. The spatial pattern of glacier retreat is markedly different. The retreat occurs more slowly for HB_{M19} and HB_{HF12} than for HB_{ref} (Figs 8, 9a). In these cases, the larger frontal mass loss at HB_{ref} due to correct water depths at the glacier front is outweighed by slightly larger surface mass losses at HB_{M18} and HB_{HF12} due to a longer preservation of their lower tongues, which is induced by the initially land-terminating glacier fronts.

Finally, it has to be borne in mind that long-term, i.e. centennial-scale projections which allow for the glacier to disappear completely inevitably lead to bedrock-related differences in absolute cumulative total mass loss, as the different 3-D ice bodies representing the same glacier hold different sea level-relevant ice volumes.

Conclusions

We carried out a conceptual modelling study regarding future mass loss from the tidewater glacier Hansbreen in Svalbard. In the study, Hansbreen was treated as a test-case glacier whose retreat was projected for a 500 year period using a glacier-evolution model that employs a flotation-criterion approach. Model forcing was provided by prescribed CMB profiles. Our study focused on analysing the sensitivity of mass loss from the glacier to five different choices of bedrock topography. One of those bedrocks had been derived from extensive ground-penetrating radar measurements, while the other four had been modelled. The study also considered different flotation characteristics for the glacier tongue and took into account five different experiments regarding the CMB forcing.

Compared with reference cumulative total mass loss from model runs that used the measured bedrock and ice thickness (HB_{ref}), we found that the characteristic overestimation of bedrock elevations towards the glacier front in the modelled bedrock datasets (and the related underestimation of ice thickness) leads to a time lag in mass losses from the glacier front that lies in the range of 16 (HB_{M22}) to 75 years (HB_{HF12}) depending on the respective bedrock dataset. Related to this time lag we found a similar underestimation of cumulative total mass loss over the first couple of decades of the modelling period when using any of the modelled bedrock datasets. Size and temporal extent of this underestimation vary between datasets. On the longer term, i.e. after the initial common underestimation, deviations in cumulative total mass loss develop according to varying bedrock depth, which implies considerable overestimations for deeper bedrocks.

Under warmer climate scenarios, the initial underestimation of total mass loss is reduced substantially. In case of a floating glacier tongue (which concerns only a minority of tidewater glaciers), this reduction is, however, counterbalanced by the sensitivity of total mass loss to flotation characteristics. Preservation of a floating tongue is less likely in warmer climates. As for grounded tongues the initial underestimation is larger and develops faster than for floating tongues, this might reduce the effect that climate warming has on the initial underestimation of total mass loss.

Accordingly, the time lag in mass losses from the glacier front shrinks to 14–35 years (depending on the chosen bedrock dataset) under Ex_{2b} forcing (which resembles RCP 8.5 conditions), when observed flotation characteristics ($\beta=1.15$) are assumed. Comparing the different cumulative total mass-loss trajectories and their under-/overestimation patterns suggests the modelled

bedrock/ice thickness dataset of Millan and others (2022) (HB_{M22}) as the most suitable alternative for future glacier evolution modelling. For this 3-D ice body representation of Hansbreen the maximum underestimation of cumulative total mass loss at the beginning of the modelling period is limited to 2.9% (0.2 Gt) under an RCP 8.5 conditions. All other modelled 3-D ice bodies considered in our study show an underestimation of cumulative total mass loss by $\sim 10\%$.

The bedrock topography influences the trajectories of all types of mass loss. Water depth at the calving front determines the size of the flux gate and controls the timing of frontal retreat together with the chosen flotation parameter. Hereby, the influence of different bedrock topographies on cumulative total mass loss and its partitioning is distinctly larger than that of the chosen flotation parameter. In the control run (reference 3-D ice body (HB_{ref}), constant present CMB (Ex_0), observed flotation parameter ($\beta = 1.15$)), cumulative total mass loss of Hansbreen is dominated by contributions of CMB (57%) and calving flux (42%). Contributions of frontal retreat are of minor importance (1%) for total mass loss. This partitioning between surface mass loss and mass loss at the glacier front is substantially different under RCP 8.5 conditions (87% vs 13%), with bedrock/ice thickness characteristics exerting further, considerable influence. In case of deeper bedrocks with higher submarine ice volumes than those of the reference 3-D ice body (HB_{ref}), the shares of mass loss at the glacier front are distinctly higher (65/76% vs 35/24% for HB_{F14} and HB_{M22} , respectively). In case of shallower bedrocks, the shares of mass loss at the glacier front are almost negligible (98/96% vs 2/4% for HB_{HF12} and HB_{M19} , respectively).

Taken together, our findings suggest that under the influences of warmer climates accurate bedrock/ice thickness data are especially important for future glacier evolution modelling on decadal timescales, over which most of the differences in sea level-relevant mass loss unfold. Flotation characteristics of the glacier tongue during its marine-terminating phase are of additional but minor importance. Hence, with ongoing atmospheric warming the need for reliable input data and accurate parameterizations in tidewater glacier projections in fact increases further.

Acknowledgements. This study was funded by grants no. 03F0778D and 03F0855B of the German Federal Ministry of Education and Research (BMBF). Additional funding was provided by grant no. MA 6966/6-1 of the German Research Foundation (DFG). Parts of the preparatory work had been financed by grant no. MO2653/1-2 of the DFG. The contribution of FN was supported by grant PID2020-113051RB-C31 from Agencia Estatal de Investigación. Modelled ice thickness data were obtained from the ETH Zürich research collection repository (doi:10.3929/ethz-b-000315707).

References

- Åkesson H, Nisancioglu KH and Nick FM (2018) Impact of fjord geometry on grounding line stability. *Frontiers in Earth Science* **6**, 71. doi: [10.3389/feart.2018.00071](https://doi.org/10.3389/feart.2018.00071)
- Benn DI and Åström JA (2018) Calving glaciers and ice shelves. *Advances in Physics: X* **3**(1), 1513819. doi: [10.1080/23746149.2018.1513819](https://doi.org/10.1080/23746149.2018.1513819)
- Benn DI, Warren CR and Mottram RH (2007) Calving processes and the dynamics of calving glaciers. *Earth-Science Reviews* **82**, 143–179. doi: [10.1016/j.earscirev.2007.02.002](https://doi.org/10.1016/j.earscirev.2007.02.002)
- Błaszczak M, Jania JA and Hagen JO (2009) Tidewater glaciers of Svalbard: recent changes and estimates of calving fluxes. *Polish Polar Research* **30**(2), 85–142.
- Błaszczak M, Jania JA and Kolondra L (2013) Fluctuations of tidewater glaciers in Hornsund fjord (southern Svalbard) since the beginning of the 20th century. *Polish Polar Research* **34**(4), 327–352. doi: [10.2478/popore-2013-0024](https://doi.org/10.2478/popore-2013-0024)
- Brown CS, Meier MF and Post A (1982) Calving speed of Alaska tidewater glaciers, with application to Columbia Glacier. *USGS Prof. Pap.* 1258-C, C1–C13. doi: [10.3133/pp1258c](https://doi.org/10.3133/pp1258c)
- Catania GA and 7 others (2018) Geometric controls on tidewater glacier retreat in central western Greenland. *Journal of Geophysical Research: Earth Surface* **123**, 2024–2038. doi: [10.1029/2017JF004499](https://doi.org/10.1029/2017JF004499)
- Choi Y, Morlighem M, Wood M and Bondzio JH (2018) Comparison of four calving laws to model Greenland outlet glaciers. *The Cryosphere* **12**, 3735–3746. doi: [10.5194/tc-12-3735-2018](https://doi.org/10.5194/tc-12-3735-2018)
- Cogley JG and 10 others (2011) Glossary of glacier mass balance and related terms (IHP-VII Technical Documents in Hydrology No. 86, IACS Contribution No. 2), UNESCO–IHP, Paris.
- Ćwiakła J and 5 others (2018) Submarine geomorphology at the front of the retreating Hansbreen tidewater glacier, Hornsund fjord, southwest Spitsbergen. *Journal of Maps* **14**(2), 123–134. doi: [10.1080/17445647.2018.1441757](https://doi.org/10.1080/17445647.2018.1441757)
- De Andrés E and 5 others (2018) A two-dimensional glacier–fjord coupled model applied to estimate submarine melt rates and front position changes of Hansbreen, Svalbard. *Journal of Glaciology* **64**(247), 745–758. doi: [10.1017/jog.2018.61](https://doi.org/10.1017/jog.2018.61)
- De Andrés E, Otero J, Navarro FJ and Walczowski W (2021) Glacier-plume or glacier-fjord circulation models? A 2-D comparison for Hansbreen–Hansbukta system, Svalbard. *Journal of Glaciology* **67**(265), 797–810. doi: [10.1017/jog.2021.27](https://doi.org/10.1017/jog.2021.27)
- Enderlin EM, Howat IM and Vieli A (2013) High sensitivity of tidewater outlet glacier dynamics to shape. *The Cryosphere* **7**(3), 1007–1015. doi: [10.5194/tc-7-1007-2013](https://doi.org/10.5194/tc-7-1007-2013)
- Farinotti D and 36 others (2017) How accurate are estimates of glacier ice thickness? Results from ITMIX, the Ice Thickness Models Intercomparison eXperiment. *The Cryosphere* **11**(2), 949–970. doi: [10.5194/tc-11-949-2017](https://doi.org/10.5194/tc-11-949-2017)
- Farinotti D and 6 others (2019) A consensus estimate of the ice thickness distribution of all glaciers on Earth. *Nature Geoscience* **12**, 168–173. doi: [10.1038/s41561-019-0300-3](https://doi.org/10.1038/s41561-019-0300-3)
- Farinotti D, Huss M, Bauder A and Funk M (2009) A method to estimate the ice volume and ice-thickness distribution of alpine glaciers. *Journal of Glaciology* **55**(191), 422–430. doi: [10.3189/002214309788816759](https://doi.org/10.3189/002214309788816759)
- Frank T, Åkesson H, de Fleurian B, Morlighem M and Nisancioglu KH (2022) Geometric controls of tidewater glacier dynamics. *The Cryosphere* **16**(2), 581–601. doi: [10.5194/tc-16-581-2022](https://doi.org/10.5194/tc-16-581-2022)
- Frey H and 9 others (2014) Estimating the volume of glaciers in the Himalayan–Karakoram region using different methods. *The Cryosphere* **8**, 2313–2333. doi: [10.5194/tc-8-2313-2014](https://doi.org/10.5194/tc-8-2313-2014)
- Fürst JJ and 25 others (2018) The ice-free topography of Svalbard. *Geophysical Research Letters* **45**(21), 11760–11769. doi: [10.1029/2018GL079734](https://doi.org/10.1029/2018GL079734)
- GlaThiDa Consortium (2019) *Glacier Thickness Database 3.0.1*. Zurich, Switzerland: World Glacier Monitoring Service. doi: [10.5904/wgms-glathida-2019-03](https://doi.org/10.5904/wgms-glathida-2019-03)
- Grabiec M, Jania JA, Puczek D, Kolondra L and Budzik T (2012) Surface and bed morphology of Hansbreen, a tidewater glacier in Spitsbergen. *Polish Polar Research* **33**(2), 111–138. doi: [10.2478/v10183-012-0010-7](https://doi.org/10.2478/v10183-012-0010-7)
- Hanson B and Hooke RL (2000) Glacier calving: a numerical model of forces in the calving-speed/water-depth relation. *Journal of Glaciology* **46**(153), 188–196. doi: [10.3189/172756500781832792](https://doi.org/10.3189/172756500781832792)
- Hock R and 7 others (2019) GlacierMIP – a model intercomparison of global-scale glacier mass-balance models and projections. *Journal of Glaciology* **65**(251), 453–467. doi: [10.1017/jog.2019.22](https://doi.org/10.1017/jog.2019.22)
- Hugonnet R and 10 others (2021) Accelerated global glacier mass loss in the early twenty-first century. *Nature* **592**, 726–731.
- Huss M and Farinotti D (2012) Distributed ice thickness and volume of all glaciers around the globe. *Journal of Geophysical Research* **117**(F4), F04010. doi: [10.1029/2012JF002523](https://doi.org/10.1029/2012JF002523)
- Huss M and Hock R (2015) A new model for global glacier change and sea-level rise. *Frontiers in Earth Science* **3**, 54. doi: [10.3389/feart.2015.00054](https://doi.org/10.3389/feart.2015.00054)
- Huss M, Stöckli R, Kappenberger G and Blatter H (2008) Temporal and spatial changes of Laika Glacier, Canadian Arctic, since 1959, inferred from satellite remote sensing and mass-balance modelling. *Journal of Glaciology* **54**(188), 857–866. doi: [10.3189/00221430878779979](https://doi.org/10.3189/00221430878779979)
- Jakobsson M and Mayer LA (2022) Polar region bathymetry: critical knowledge for the prediction of global sea level rise. *Frontiers in Marine Science* **8**, 788724. doi: [10.3389/fmars.2021.788724](https://doi.org/10.3389/fmars.2021.788724)
- Jania J, Mochnacki D and Gądek B (1996) The thermal structure of Hansbreen, a tidewater glacier in southern Spitsbergen, Svalbard. *Polish Polar Research* **15**(1), 53–66. doi: [10.3402/polar.v15i1.6636](https://doi.org/10.3402/polar.v15i1.6636)
- Linsbauer A, Paul F and Haerberli W (2012) Modeling glacier thickness distribution and bed topography over entire mountain ranges with GlabTop:

- application of a fast and robust approach. *Journal of Geophysical Research* **117**(F3), F03007. doi: [10.1029/2011JF002313](https://doi.org/10.1029/2011JF002313)
- Luckman A and 5 others** (2015) Calving rates at tidewater glaciers vary strongly with ocean temperature. *Nature Communications* **6**, 8566. doi: [10.1038/ncomms9566](https://doi.org/10.1038/ncomms9566)
- Mankoff KD and 5 others** (2020) Greenland ice sheet solid ice discharge from 1986 through March 2020. *Earth System Science Data* **12**, 1367–1383. doi: [10.5194/essd-12-1367-2020](https://doi.org/10.5194/essd-12-1367-2020)
- Marzeion B and 16 others** (2020) Partitioning the uncertainty of ensemble projections of global glacier mass change. *Earth's Future* **8**(7), e2019EF001470. doi: [10.1029/2019EF001470](https://doi.org/10.1029/2019EF001470)
- Maussion F and 14 others** (2019) The Open Global Glacier Model (OGGM) v1.1. *Geoscientific Model Development* **12**(3), 909–931. doi: [10.5194/gmd-12-909-2019](https://doi.org/10.5194/gmd-12-909-2019)
- McNabb RW, Hock R and Huss M** (2015) Variations in Alaska tidewater glacier frontal ablation, 1985–2013. *Journal of Geophysical Research: Earth Surface* **120**(1), 120–136. doi: [10.1002/2014JF003276](https://doi.org/10.1002/2014JF003276)
- Millan R, Mouginot J, Rabatel A and Morlighem M** (2022) Ice velocity and thickness of the world's glaciers. *Nature Geoscience* **15**, 124–129. doi: [10.1038/s41561-021-00885-z](https://doi.org/10.1038/s41561-021-00885-z)
- Möller M, Friedl P, Palmer SJ and Marzeion B** (2022) Grounding line retreat and ice discharge variability at two surging, ice shelf-forming basins of Flade Isblink ice cap, northern Greenland. *Journal of Geophysical Research: Earth Surface* **127**(2), e2021JF006302. doi: [10.1029/2021JF006302](https://doi.org/10.1029/2021JF006302)
- Möller M and Kohler J** (2018) Differing climatic mass balance evolution across Svalbard glacier regions over 1900–2010. *Frontiers in Earth Science* **6**, 128. doi: [10.3389/feart.2018.00128](https://doi.org/10.3389/feart.2018.00128)
- Möller M and Möller R** (2017) Modeling glacier-surface albedo across Svalbard for the 1979–2015 period: the HiRSvαC500-α data set. *Journal of Advances in Modeling Earth Systems* **9**, 404–422. doi: [10.1002/2016MS000752](https://doi.org/10.1002/2016MS000752)
- Möller M, Navarro F and Martín-Español A** (2016a) Monte Carlo modelling projects the loss of most land-terminating glaciers on Svalbard in the 21st century under RCP 8.5 forcing. *Environmental Research Letters* **11**, 094006. doi: [10.1088/1748-9326/11/9/094006](https://doi.org/10.1088/1748-9326/11/9/094006)
- Möller M and 5 others** (2016b) Adjustment of regional climate model output for modeling the climatic mass balance of all glaciers on Svalbard. *Journal of Geophysical Research: Atmospheres* **121**(10), 5411–5429. doi: [10.1002/2015JD024380](https://doi.org/10.1002/2015JD024380)
- Moore JC, Grinsted A, Zwinger T and Jevrejeva S** (2013) Semi-empirical and process-based global sea level projections. *Reviews of Geophysics* **51**(3), 484–522. doi: [10.1002/rog.20015](https://doi.org/10.1002/rog.20015)
- Navarro FJ and 6 others** (2014) Ice volume estimates from ground-penetrating radar surveys, Wedel Jarlsberg land glaciers, Svalbard. *Arctic, Antarctic, and Alpine Research* **46**(2), 394–406. doi: [10.1657/1938-4246-46.2.394](https://doi.org/10.1657/1938-4246-46.2.394)
- Nick FM and 7 others** (2013) Future sea-level rise from Greenland's main outlet glaciers in a warming climate. *Nature* **497**, 235–238. doi: [10.1038/nature12068](https://doi.org/10.1038/nature12068)
- Norwegian Polar Institute** (2014) *Terrengmodell Svalbard (S0 Terrengmodell) [Data set]*. Norwegian Polar Institute. <https://data.npolar.no/dataset/dce53a47-c726-4845-85c3-a65b46fe2fea>.
- Oerlemans J, Jania J and Kolondra L** (2011) Application of a minimal glacier model to Hansbreen, Svalbard. *The Cryosphere* **5**(1), 1–11. doi: [10.5194/tc-5-1-2011](https://doi.org/10.5194/tc-5-1-2011)
- Oerlemans J and Nick FM** (2005) A minimal model of a tidewater glacier. *Annals of Glaciology* **42**, 1–6. doi: [10.3189/172756405781813023](https://doi.org/10.3189/172756405781813023)
- Otero J and 5 others** (2017) Modeling the controls on the front position of a tidewater glacier in Svalbard. *Frontiers in Earth Science* **5**, 29. doi: [10.3389/feart.2017.00029](https://doi.org/10.3389/feart.2017.00029)
- Pelto MS and Warren CR** (1991) Relationship between tidewater glacier calving velocity and water depth at the calving front. *Annals of Glaciology* **15**, 115–118. doi: [10.3189/S0260305500009617](https://doi.org/10.3189/S0260305500009617)
- Pętllicki M, Ciepły M, Jania J, Promińska A and Kinnard C** (2015) Calving of a tidewater glacier driven by melting at the waterline. *Journal of Glaciology* **61**(229), 851–863. doi: [10.3189/2015JG15J062](https://doi.org/10.3189/2015JG15J062)
- Pfeffer WT and 19 others** (2014) The Randolph Glacier Inventory: a globally complete inventory of glaciers. *Journal of Glaciology* **60**(221), 537–552. doi: [10.3189/2014JG13J176](https://doi.org/10.3189/2014JG13J176)
- Porter C and 28 others** (2018) ArcticDEM. doi: [10.7910/DVN/OHHUKH](https://doi.org/10.7910/DVN/OHHUKH)
- Rabatel A, Sanchez O, Vincent C and Six D** (2018) Estimation of glacier thickness from surface mass balance and ice flow velocities: a case study on Argentière Glacier, France. *Frontiers in Earth Science* **6**, 112. doi: [10.3389/feart.2018.00112](https://doi.org/10.3389/feart.2018.00112)
- Recinos B, Maussion F, Noël B, Möller M and Marzeion B** (2021) Calibration of a frontal ablation parameterisation applied to Greenland's peripheral calving glaciers. *Journal of Glaciology* **67**(266), 1177–1189. doi: [10.1017/jog.2021.63](https://doi.org/10.1017/jog.2021.63)
- Recinos B, Maussion F, Rothenpieler T and Marzeion B** (2019) Impact of frontal ablation on the ice thickness estimation of marine-terminating glaciers in Alaska. *The Cryosphere* **13**, 2657–2672. doi: [10.5194/tc-13-2657-2019](https://doi.org/10.5194/tc-13-2657-2019)
- Sánchez-Gómez P and 5 others** (2019) Intra- and inter-annual variability in dynamic discharge from The Academy of Sciences Ice Cap, Severnaya Zemlya, Russian Arctic, and its role in modulating mass balance. *Journal of Glaciology* **65**(253), 780–797. doi: [10.1017/jog.2019.58](https://doi.org/10.1017/jog.2019.58)
- Schäfer M, Möller M, Zwinger T and Moore JC** (2015) Dynamic modelling of future glacier changes: mass-balance/elevation feedback in projections for the Vestfonna Ice Cap, Nordaustlandet, Svalbard. *Journal of Glaciology* **61**(230), 1121–1136. doi: [10.3189/2015JG14J184](https://doi.org/10.3189/2015JG14J184)
- Schoof C** (2007) Ice sheet grounding line dynamics: steady states, stability, and hysteresis. *Journal of Geophysical Research* **112**, F03S28. doi: [10.1029/2006JF000664](https://doi.org/10.1029/2006JF000664)
- van der Veen CJ** (1996) Tidewater calving. *Journal of Glaciology* **42**(141), 375–385. doi: [10.3189/S0022143000004226](https://doi.org/10.3189/S0022143000004226)
- van der Veen CJ** (2002) Calving glaciers. *Progress in Physical Geography* **26**(1), 96–122. doi: [10.1191/0309133302pp327ra](https://doi.org/10.1191/0309133302pp327ra)
- van Pelt W, Schuler T, Pohjola V and Pettersson R** (2021) Accelerating future mass loss of Svalbard glaciers from a multi-model ensemble. *Journal of Glaciology* **67**(263), 485–499. doi: [10.1017/jog.2021.2](https://doi.org/10.1017/jog.2021.2)
- Vaughan DG and Doake CSM** (1996) Recent atmospheric warming and retreat of ice shelves on the Antarctic Peninsula. *Nature* **379**, 328–331. doi: [10.1038/379328a0](https://doi.org/10.1038/379328a0)
- Vieli A, Funk M and Blatter H** (2000) Tidewater glaciers: frontal flow acceleration and basal sliding. *Annals of Glaciology* **31**, 217–221. doi: [10.3189/172756400781820417](https://doi.org/10.3189/172756400781820417)
- Vieli A, Funk M and Blatter H** (2001) Flow dynamics of tidewater glaciers: a numerical modelling approach. *Journal of Glaciology* **47**(159), 595–606. doi: [10.3189/172756501781831747](https://doi.org/10.3189/172756501781831747)
- Vieli A, Jania J and Kolondra L** (2002) The retreat of a tidewater glacier: observations and model calculations on Hansbreen, Spitsbergen. *Journal of Glaciology* **48**(163), 592–600. doi: [10.3189/172756502781831089](https://doi.org/10.3189/172756502781831089)
- Welty E and 11 others and GlaThiDa Contributors** (2020) Worldwide version-controlled database of glacier thickness observations. *Earth System Science Data* **12**, 3039–3055. doi: [10.5194/essd-12-3039-2020](https://doi.org/10.5194/essd-12-3039-2020)
- Zwally HJ and 5 others** (2002) Surface melt-induced acceleration of Greenland ice sheet flow. *Science* **297**(5579), 218–222. doi: [10.1126/science.1072708](https://doi.org/10.1126/science.1072708)